Summer 2017

Processing and properties of WC-based Cu-Ni-Mn-Zn metal matrix composites produced via pressureless infiltration

Paul M. Brune

Department:

PROCESSING AND PROPERTIES OF WC-BASED CU-NI-MN-ZN METAL MATRIX COMPOSITES PRODUCED VIA PRESSURELESS INFILTRATION

by

PAUL MICHAEL BRUNE

A THESIS

Presented to the Faculty of the Graduate School of the

MISSOURI UNIVERSITY OF SCIENCE AND TECHNOLOGY

In Partial Fulfillment of the Requirements for the Degree

MASTER OF SCIENCE IN CERAMIC ENGINEERING

2017

Approved by

Greg E. Hilmas, Advisor
Jeremy L. Watts
Ronald J. O'Malley

PUBLICATION THESIS OPTION

This thesis consists of the following two articles which will have been or will be submitted for publication as follows.

Paper I: Pages 22-39 entitled "The Wetting of TaC, B_4C, WC, and SiC by Cu-Ni-Mn and Cu-Ni-Mn-Zn Alloys" are intended for submission to the Journal of the American Ceramic Society.

Paper II: Pages 40-57 entitled "The Processing and Properties of WC-based/Cu-Ni-Mn-Zn Metal Matrix Composites" are intended for submission to the Journal of the American Ceramic Society.

ABSTRACT

This research focuses on the processing and properties of tungsten carbide-based (WC-based) Cu-Ni-Mn-Zn metal matrix composites (MMCs) fabricated by pressureless infiltration. The first goal of this project was to test the wettability of Cu-Ni-Mn and Cu-Ni-Mn-Zn on various carbides. The sessile drop technique was employed to determine if they were suitable candidates for pressureless infiltration. The carbides investigated were TaC, WC, B_4C, and SiC. It was determined that both alloys had contact angles of less than 70° on TaC, WC, and B_4C, which is one requirement for pressureless infiltration. However, both alloys reacted with B_4C to produce graphite at the metal-ceramic interface. Since graphite is not wet by either alloy, the presence of graphite disqualified B_4C as a candidate for pressureless infiltration. The second goal of the project was to establish a baseline for the hardness, transverse rupture strength (TRS), fracture toughness, and wear resistance of WC/Cu-Ni-Mn-Zn MMCs and examine the effect of substituting 10 vol. % of WC for VC, cBN, and TaC on the microstructure and mechanical properties. The baseline hardness, TRS, fracture toughness, and wear resistance were measured to be 3.3 ± 0.2 GPa, 838 ± 61 MPa, 20.7 ± 0.4 MPa•$m^{1/2}$, and 20.8 ± 4.6 mm^3, respectfully. The substitution of VC and cBN increased the porosity of the microstructure while decreasing hardness and TRS. The substitution of TaC also increased the porosity, but to a lesser extent as well as having little effect on the hardness resulting in a higher TRS with the TaC10 composition measuring 1000 ± 47 MPa. The substitution of VC and TaC increased the fracture toughness with the TaC3 composition measuring highest at 26.5 ± 0.3 MPa•$m^{1/2}$. However, both the VC and the TaC10 compositions had a higher volume loss than the baseline in wear testing.

ACKNOWLEDGEMENTS

First, I would like to thank my advisor, Dr. Gregory Hilmas, for his guidance and patience over the past two years. Without his council, I would have never considered becoming a ceramic engineer, and it was with his council that I, in part, decided to become a graduate student. I thank him for allowing me the opportunity to travel the country to present my research. Most of all, I would like to thank him for the opportunities and advice that he provided to me for teaching undergraduates both in the lab and in the classroom. Next, I would like to thank Dr. Jeremy Watts for his invaluable assistance in the laboratory and in writing. Without his guidance, I would have never made it through the past two years. I would also be considerably worse at racquetball. Thank you also to Dr. Fahrenholtz and Dr. O'Malley who provided me the tools and direction to pursue my research into the field of wetting and metal-ceramic interactions.

Thank you to my peers in 307 for all of your help and support. They taught me how to operate much of the equipment necessary for my research and helped me build the equipment that was needed. They kept me on track when I needed it most, provided sound advice, and added to my understanding of ceramic processing. Thank you also to all the undergraduate researchers who contributed to this body of research, your help and input was invaluable.

Finally, I would like to thank my family and my friends for always believing in me throughout the years. You are the source of my strength during long nights and the source of my inspiration when times get rough. Without you all, I would not have made it to where I am today. Thank you.

TABLE OF CONTENTS

Page

LIST OF ILLUSTRATIONS

PAPER II

LIST OF TABLES

1. INTRODUCTION

The development of metal matrix composites (MMCs) is critical to the tooling, mining, and abrasives industries.[1, 2, 3] MMCs are made to take advantage of the hardness of the ceramic phase and the toughness of the metal phase in order to produce a composite with both attributes.[4] There are many types of MMCs that are used in each industry, but tungsten carbide cobalt-based (WC/Co-based) MMCs are by far the most prevalent.[1, 3, 5] WC/Co-based MMCs boast a wide range of material properties with hardness ranging from 8 GPa to 24 GPa, toughness ranging from 7 MPa•$m^{1/2}$ to 25 MPa•$m^{1/2}$ and transverse rupture strength ranging from 2 GPa to 3 GPa.[1, 4, 6]

One requirement for the successful production of MMCs is the wettability between the metal alloy and the ceramic. The sessile drop method is one process by which the contact angle, and thus the wettability of a liquid metal on a ceramic substrate, can be determined. The application of this technique for liquid metals on ceramic substrates is common in the technical literature.[7, 8, 9] The main MMC production route used in this body of research is pressureless infiltration, which is the process of a metal alloy penetrating into a ceramic powder bed or preform without the use of outside force. This method requires a threshold contact angle of 70° to 80° between the metal and the ceramic.[10]

For the past few decades there has been substantial research into a replacement material for either tungsten carbide as a hard-reinforcing phase or cobalt as the soft binder phase due to factors such as cost and availability.[3] One such family of binder metal alloys is Cu-Ni-Mn which has been used in brazing, hard facing, and the

production of metal matrix composites in recent studies.[11, 12, 13] One of the most attractive properties of Cu-Ni-Mn-Zn in particular is the wettability of tungsten carbide, allowing for pressureless (spontaneous) infiltration.[12]

The purpose of this research has been to expand upon the currently known microstructural and mechanical properties of tungsten carbide Cu-Ni-Mn-Zn MMCs as well as determining other ceramic materials that can be used with Cu-Ni-Mn-Zn in order to achieve spontaneous infiltration. This research addresses the following questions:

1. What other ceramic materials that have hardness ≥ 20 GPa are wet by Cu-Ni-Mn or Cu-Ni-Mn-Zn in a manner that would allow for spontaneous infiltration?

2. What are the baseline mechanical properties of tungsten carbide Cu-Ni-Mn-Zn MMCs produced by spontaneous infiltration?

3. How does the substitution of 10 vol. % vanadium carbide, cubic boron nitride, or tantalum carbide for tungsten carbide change the microstructure and mechanical properties of tungsten carbide Cu-Ni-Mn-Zn MMCs produced by spontaneous infiltration?

As a whole, the research described in this thesis has the potential to improve upon the current knowledge of copper based tungsten carbide MMCs and the factors that influence the production of MMCs by spontaneous infiltration.

2. LITERATURE REVIEW

2.1. PROPERTIES OF BASE MATERIALS

Metal matrix composites consist of a ceramic particulate and a metal binder alloy. This section will outline the crystalline structure and some mechanical properties of the various ceramics used in this study as well as the two binder metal alloys. Each of the ceramic materials were selected for testing due to their high hardness, and previous use in other metal matrix composites, particularly cobalt – based and copper – based.

2.1.1. Tungsten Carbide. Tungsten carbide is a high-hardness, ceramic material that is used extensively in the mining, drilling, and abrasives industries.[1, 3, 4] Figure 2.1 shows the hexagonal crystal structure of tungsten monocarbide which belongs to the $P\bar{6}m2$ space group.[14] Currently there is a push to effectively produce dense specimens of "binderless" tungsten carbide through spark plasma sintering (SPS) for a variety of applications including waterjet nozzles.[15, 16, 17] However, the majority of the market for tungsten carbide is for the manufacturing of metal matrix composites (MMCs).[1, 3, 4] While the majority of tungsten carbide MMCs are cobalt-based there has been research into using various other metals for the matrix material including copper, iron, and nickel.[3, 18, 19, 20] The use of tungsten carbide in metal matrix composites works to combine the hardness and stiffness of tungsten carbide with the ductility of the metal binder.[3] The hardness of tungsten carbide has been reported to be in the range of 27 – 34 GPa and the Young's modulus is around 500 - 700 GPa.[14, 15]

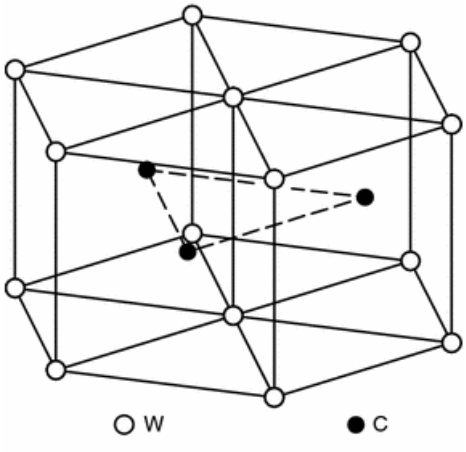

Figure 2.1. The hexagonal crystal structure of WC, space group P$\bar{6}$m2. Adapted from Kurlov et al.[21]

2.1.2. Tantalum Carbide. Tantalum carbide is an ultra-high temperature and wear resistant ceramic material with applications in both high-speed tooling and aerospace.[22, 23] Tantalum carbide has a cubic crystal structure of the NaCl type which has the space group F$m\bar{3}m$ as shown in Figure 2.2.[14, 24] Though the material can be produced by pressureless sintering, the bulk of the literature has focused on hot-pressing for fabrication.[22, 25] Typical hot-pressing parameters for TaC involve pressing at a temperature between 1900°C and 2400°C and pressure of 30 MPa in an argon or helium atmosphere depending on the hold temperature.[22] The melting point of tantalum carbide is higher than most materials at around 3900°C.[23] The hardness of tantalum carbide has been reported in the range of 15 – 20 GPa.[22, 24, 25] Tantalum carbide can also be used in MMCs. The main role of tantalum carbide in current tungsten carbide cobalt-based (WC/Co-based) MMCs is as a grain growth inhibitor.[1, 26]

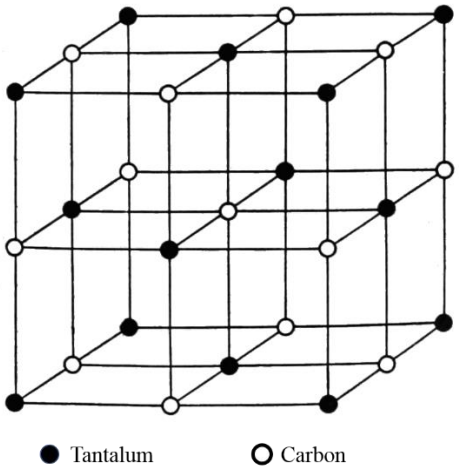

Figure 2.2. The cubic crystalline structure of tantalum carbide space group Fm$\bar{3}$m.

2.1.3. Vanadium Carbide. Vanadium carbide is a hard and brittle transition metal carbide known for its use as a precipitant in hardened steels and as an additive in MMCs.[1, 27, 28] The structure of vanadium carbide is also cubic of the NaCl type shown in Figure 2.2.[14, 29] While not often used as a monolithic solid, vanadium carbide is often added to other materials due to its high hardness (19 - 25 GPa) and grain growth inhibiting properties.[1, 30, 31] While vanadium carbide has been shown to be one of the most effective grain growth inhibiting species in WC/Co-based MMCs it has also lead to the embrittlement of the microstructure when used alone.[1] Therefore, vanadium carbide is often added in the presence of other grain-growth inhibiting carbides, such as chromium or tantalum carbide.[1]

2.1.4. Silicon Carbide. Silicon carbide is classified as an advanced structural ceramic that is often used for high temperature and aggressive environments.[32] The hardness, strength, and wear resistance of silicon carbide lead to its use in a variety of

applications such as gas turbines, abrasives, and armor.[32, 33, 34] The crystalline structure of α-silicon carbide is hexagonal.[14] Silicon carbide is also widely used in ceramic matrix composites (CMCs) and MMCs. SiC-SiC composites are currently being researched and developed for use in aerospace, specifically for jet turbine engines.[35, 36] Silicon carbide is often chosen for use in fiber and particle reinforced MMC's for its high hardness and low cost. There is currently research on using silicon carbide as a reinforcement phase for alloys of iron, copper, nickel, and aluminum as well as many others.[37, 38, 39, 40] The hardness of silicon carbide has been reported to be in the range of 19 – 29 GPa depending on the processing route and the sintering additives.[32, 33, 41] The flexure strength of silicon carbide has been reported to be around 420 MPa.[14, 33]

2.1.5. Boron Carbide. Boron carbide is a ceramic compound known for its high hardness, high melting temperature, chemical stability, low density, and high neutron absorption cross section.[42, 43, 44, 45] Boron carbide belongs to the D_{3d^5} - ($R\bar{3}m$) space group with a rhombohedral crystal structure consisting of 15 atoms corresponding to $B_{12}C_3$.[29, 43] Figure 2.3 shows the crystalline structure of boron carbide and features the $B_{11}C$ icosahedra connected by C-B-C chains. Boron carbide can be sintered pressurelessly with the use of additives including Cr, Co, amorphous carbon, and TiB_2 among others.[45, 46] Another method of boron carbide fabrication is by hot pressing. Typical hot press parameters for boron carbide involve temperatures of 2000°C to 2200°C, pressures of 15 to 40 MPa, and 15 to 45 min hold times in graphite dies.[43, 47, 48]

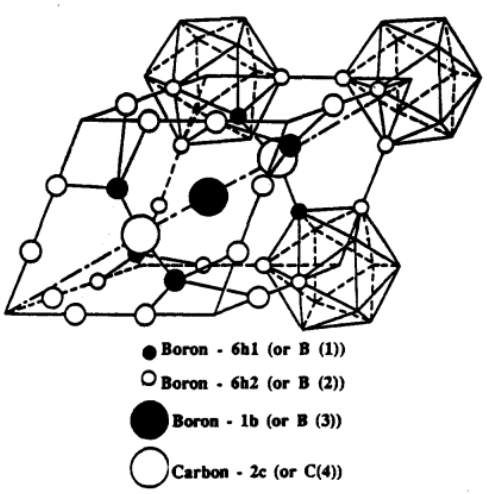

Figure 2.3. The rhombohedral crystalline structure of boron carbide. Adapted from Thevenot et al..[43]

The mechanical and chemical properties of boron carbide make it a useful material for the nuclear, mining, and abrasive industries. A study by Maruyama et al. explored the possibility of producing a copper-based boron carbide metal matrix composite for use in Liquid-Metal-Cooled Fast Breeder Reactors.[42] The density of boron carbide is lower than that of many other hard ceramic materials at 2.52 g/cm^3 making it desirable in the manufacturing of armour.[47] The mining and abrasive industries are implementing boron carbide into their products due to high hardness and wear resistance. The hardness of boron carbide has been reported to be in the range of 14 – 38 GPa depending on sintering process, final density, purity, and test method.[43, 45, 46, 47] The wear resistance of boron carbide has been a determining factor in its selection for a reinforcing particle in aluminum matrix composites.[49]

2.1.6. Cubic Boron Nitride. Cubic boron nitride is a high-temperature and high-pressure allotrope of boron nitride. While hexagonal boron nitride is soft and generally used as a high temperature lubricant, cubic boron nitride is hard and used as an abrasive material similar to diamond.[50, 51] The crystalline structure of cubic boron nitride is the same as diamond, zincblende, just as the crystal structures for hexagonal boron nitride and graphite are the same.[52] The crystalline structure of cubic boron nitride is shown in Figure 2.4. Cubic boron nitride was first synthesized by Wentorf in 1957 using a double-ended conical piston apparatus designed by Hall.[51, 53] The required temperature and pressure to synthesize cubic boron nitride using this method was 2500°C and 4 GPa.[51] The hardness of cubic boron nitride has been reported to be around 60 – 75 GPa.[52] Presently, there is research into using cubic boron nitride as reinforcement phase and as a coating in iron, cobalt, and nickel containing MMCs due to its chemical stability and hardness.[54, 55, 56]

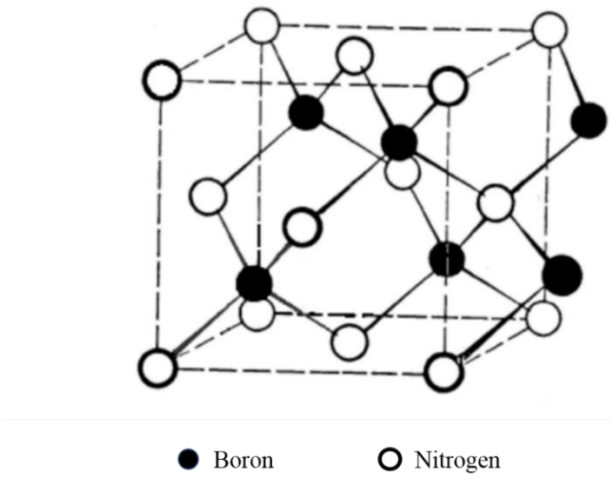

Figure 2.4. The zincblende crystalline structure of cubic boron nitride.

2.1.7. Cu-Ni-Mn-Zn and Cu-Ni-Mn. Cu-Ni-Mn and Cu-Ni-Mn-Zn are copper based alloys used in hardfacing, brazing, and metal matrix composites.[11, 12, 13] Cu-Ni-Mn alloys are used primarily because of their chemical compatibility with tungsten carbide and their ability to undergo precipitation hardening.[13] The use of these alloys in literature is limited as most of the information is in the form trade secrets and patent law.[57, 58, 59, 60] Liu et al. has determined the crystalline structure of the Cu-Ni-Mn braze to be face centered cubic and that the manganese and nickel have gone into solid solution with copper.[13]

2.2. WETTABILITY AND THE RELATION TO INFILTRATION

The contact angle between a liquid and a solid can be defined by Young's equation, Equation 1

$$\gamma_{sv} - \gamma_{sl} = \gamma_{lv}\cos(\theta) \tag{1}$$

where γ_{sv}, γ_{sl}, and γ_{lv} are the surface energies between the solid-vapor, solid-liquid, and liquid-vapor phases and θ is the contact angle between the liquid and the solid.[61] Young's equation is valid for the equilibrium contact angle between a solid and a liquid and does not take into account the kinetics of the formation of the interface or any reactions. This contact angle can be used as a measure of the degree of wetting between a liquid and a solid. Wettability can be measured by sessile drop, thin film stability, and resistive film breakthrough pressure experiments.[62, 63, 64, 65, 66] The sessile drop method has been used to determine the contact angle and thus the wettability of a liquid metal on a ceramic substrate. The application of this technique for liquid metals on ceramic substrates is common in the literature.[7, 8, 9, 40, 67] In the sessile drop technique, a drop of liquid metal is

held above a ceramic substrate and is made to fall onto the surface of the substrate at a set temperature. The drop is observed until the contact angle reaches equilibrium or near equilibrium and the angle is then measured geometrically. Figure 2.5 shows a schematic of a typical cross section of a liquid-solid contact angle that would be measured in a sessile drop experiment.

For the sessile drop test to be valid the surface of the substrate must be as smooth as possible. In cases of non-wetting ($\theta > 90°$) behavior roughness can cause the angle measured to be greater than the true contact angle. This is due to the pinning of the edge of the drop preventing further spreading. However, in cases of wetting ($\theta < 90°$) roughness can cause the measured angle to be less than the true contact angle because of increased interfacial surface area.[68] The latter interaction is expressed by Wenzel's equation, Equation 2

$$\cos(\theta_w) = s_r \cos(\theta_y) \tag{2}$$

where θ_w is the measured contact angle, s_r is the ratio of surface area to planar area at the interface, and θ_y is the contact angle given by Young's equation. The sessile drop test is also sensitive to surface oxidation and must be done in vacuum or inert atmosphere if oxides will interfere in the desired measurement.[69] In the same way that this test is sensitive to surface oxidation, it is also sensitive to surface defects and must be prepared appropriately to prevent an inaccurate test.

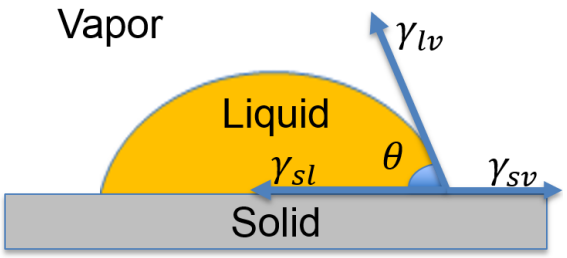

Figure 2.5. Equilibrium contact angle of a liquid on a solid substrate in cross section.

There are three main types of wetting: non-reactive or equilibrium wetting, reactive or non-equilibrium wetting, and dissolutive wetting. An example of non-reactive wetting can be observed in the Ni-40Si/SiC system. In experiments performed by Rado et al. it was shown that Ni-40Si alloy wets SiC at 1360°C without reaction.[39] Figure 2.6 shows the cross-sectional interface between Ni-40Si and SiC. While there are cooling cracks throughout the interface, the presence of an interface that is without reaction product is an indication of non-reactive wetting. One example of reactive wetting in the literature is observed in the interaction between Cu and B_4C. The cross-section of a sessile drop experiment between molten Cu and B_4C performed at 1150°C by Froumin et al. is shown in Figure 2.7. The crater in the boron carbide was determined to be the result of a reaction between Cu and B_4C resulting in the formation of a Cu-B alloy and graphite. Unlike non-reactive wetting, the drop angle changes as a function of time after contact with the surface of the substrate. Dissolutive wetting is observed between 57Bi-43Sn eutectic alloy and a pure Bi substrate. Yin et al. has explored the interactions between Bi-Sn alloys and Bi in order to explore the kinetics of wetting in that system.[70] In Figure 2.8 the interface between eutectic Bi-Sn alloy and pure Bi is observed after being held at

250°C for 12 seconds. The eutectic alloy and Bi substrate have undergone co-diffusion across the solid/liquid interface while at hold temperature without the formation of intermetallic compounds. This behavior is indicative of dissolutive wetting.[71, 72]

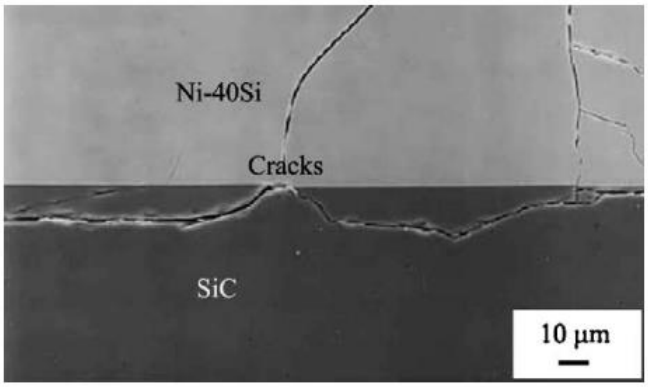

Figure 2.6. SEM micrograph of the interface between Ni-40Si metal alloy and a SiC substrate. The smooth interface is an indication of non-reactive wetting. Adapted from Rado et al. and Liu et al..[39, 40]

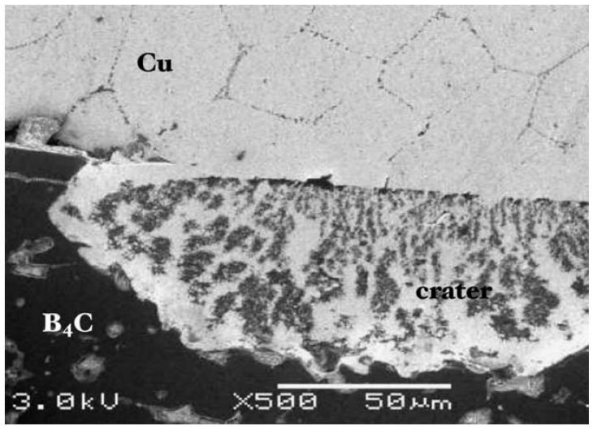

Figure 2.7. SEM micrograph of the interface between Cu and a B_4C substrate. The Cu has reacted with the B_4C resulting in a crater of Cu-B alloy (light phase) and graphite (dark phase). Adapted from Froumin et al..[73]

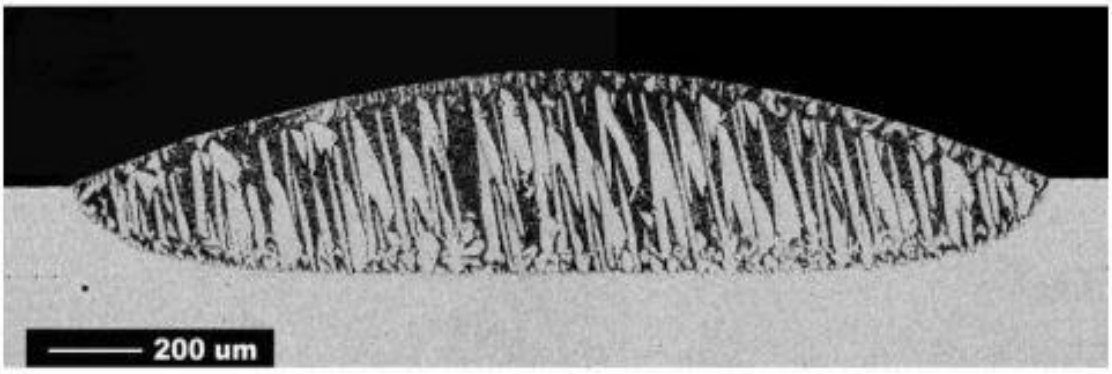

Figure 2.8. SEM micrograph of the interface between eutectic Bi-Sn alloy and pure Bi held at 250°C for 12 seconds. Adapted from Yin et al..[70]

The wettability of a metal on a ceramic can also be used as an indicator of its ability to infiltrate into a powder compact of the same ceramic. A contact angle of 90° or less is typically characterized as a wetting relationship since the energy of the system can be reduced by the spreading of the metal, thus creating more interface. However, according to Kaptay et al., the threshold contact angle for spontaneous infiltration is between 70° and 80°. While Young's equation predicts infiltration below a threshold of 90°, this does not account for the complex geometry of the pore network inside a powder compact. The equations used by Kaptay et al. account for this complex geometry. Thus, for the production of metal matrix composites via spontaneous infiltration the equilibrium contact angle would have to be lower than at least 70° and ideally as low as 0° at the processing temperature.[10] The type of wetting, reactive vs. non-reactive, and the interactions between surface oxides and the metal as well as the presence of chemical interactions between the metal and ceramic are also of importance.[7, 62] An example of this in recent literature is the case of Si infiltrating into graphite, a study by Eustathopoulous

et al. found that the reaction between silicon and carbon was the limiting factor for infiltration rate.[69] It had been thought that the infiltration was governed by a modified Washburn's equation which assumes an effective pore diameter for the powder compact and non-reactive capillary infiltration into the powder compact.[74]

In cases of non-wetting or non-infiltration between a metal and ceramic there are various methods to improve wetting and infiltration ranging from changing the chemistry of the metal to coating the ceramic in a material that is wet by the original metal.[75] In the previous example of reactive wetting between Cu and B_4C at 1150°C the contact angle was determined to be 110°.[73] This contact angle was reduced to 40° by the addition of 10.7 at.% B metal to the Cu drop. This addition was determined to have saturated the Cu with B and stopped the dissociation of B_4C at the interface, improving the wetting characteristics of the system.[73] A similar interaction was also noted between TiC_X and Cu where the wettability of the system was affected by Ti additions to the Cu metal.[76, 77] In a study by Maruyama et al. it was found that a Cu-B_4C metal matrix composite could not be produced by conventional hot pressing due to poor wetting.[42] However, after coating the surface of the B_4C powder in Cu, metal matrix composites with over 90% relative density were able to be pressed at 1050°C under a pressure of ~40 MPa for 1 hour.[42] Tariolle et al. took a different approach to successfully infiltrate B_4C with Cu that involved the addition of Si metal to the Cu.[78] The formation of graphite was determined to be the limiting factor in the inhibition of Cu infiltration into B_4C. The addition of Si was used to control the free carbon produced by the dissociation reaction between B_4C and Cu through the formation SiC. This approach significantly improved the wetting of B_4C and allowed for the infiltration of B_4C preforms.[78]

2.3. METAL MATRIX COMPOSITES

Metal matrix composites (MMCs) are composites that consist of a metal matrix with ceramic reinforcement of some type (e.g. powder or fiber reinforcement). MMCs are made to take advantage of the hardness of the ceramic phase and the toughness of the metal phase in order to produce a composite with both attributes.[4] The resulting composites have been used extensively in the tooling, mining, and abrasives industries.[2, 3] The majority of the MMC market has been dominated by tungsten carbide cobalt-based hardmetals. However, for the past few decades there has been substantial research into a replacement material for tungsten carbide as a hard-reinforcing phase or cobalt as the soft binder phase.[3] The driving forces for this research include material cost and availability, the need to reduce density in structural applications, and the desire to discover new materials for higher performance and efficiency.[3, 12, 79] Common substitutions for the cobalt matrix are aluminum, copper, nickel, and iron.[3, 19, 20, 80] Additional reinforcement materials that are being explored as replacements for tungsten carbide include titanium carbide, boron carbide, alumina, silicon nitride and silicon carbide.[3, 42, 81]

2.3.1. Processing of Metal Matrix Composites. The two main processes by which dense MMCs are produced are powder metallurgy and the infiltration of a metal into a ceramic preform.[1, 5] There are many instances in the literature where powder metallurgy is utilized to produce a dense MMC, which involves mixing ceramic and metal powders to produce a preform for densification.[80, 82] In the case where the ceramic is not wet by the metal an outside force must be applied.[10, 83] In practice this is accomplished by hot pressing or hot isostatic pressing.[42, 80] There are multiple processing options that can be utilized to this end, such as squeeze infiltration casting and high

pressure infiltration casting (HiPIC).[75] Both of these processing options have considerable drawbacks. Squeeze infiltration casting utilizes pressures in the kPA range and thus is limited to smaller and more simple geometries when used in systems without good wetting charecteristics. While HiPIC utilizes pressures of over 100 MPa to ensure infiltration of larger and more complex preforms than squeeze infiltration; the high pressure may cause damage to the reinforcing material.

The process of a metal alloy penetrating into a ceramic powder bed or preform is called infiltration. When the metal readily wets the ceramic, with an angle of 70° or less, pressureless or spontaneous infiltration may be possible.[10, 12, 19, 84] The main drawback to using spontaneous infiltration is that only a system with the previously outlined wetting characteristics, and without formation of byproducts that cause an increase in the contact angle, may be used. However, spontaneous infiltration offers a relatively fast (on the scale of hours) production cycle for near net shape complex geometries.[12, 85] Common requirements for this process are a mold that is not wet by the matrix material, a furnace that can be loaded at the temperature of infiltration, and an inert shielding gas.[12, 81, 85] The furnace and atmosphere requirements are arguably easier to satisfy over the requirements of the previously mentioned methods which sometimes include a vacuum sealed furnace with a hydraulic press.[42, 86]

2.3.2. Mechanical Properties of Metal Matrix Composites. The mechanical properties of metal matrix composites vary depending on the matrix and reinforcing materials as well as the ratio between the two. Due to the availability of information in the literature and in industry, tungsten carbide cobalt will be used for the purposes of

comparison and establishing a baseline for hardness, transverse rupture strength (TRS), elastic modulus, wear resistance, and fracture toughness.

2.3.2.1. Hardness. The hardness of metal matrix composites is typically measured either by Vickers or Rockwell indentation and reported in units of gigapascals.[1, 87, 88] While both methods of testing are valid, a Vickers hardness will be discussed in this section. ASTM C1327 gives the methodology for the standard measurement of the hardness of materials. In this method, Vickers diamond indenter is used to make an indentation on the surface of a material with a known applied force (*P*). The average diagonal of the indent (*d*) is then measured and used to calculate the hardness (HV) in GPa with Equation 3.

$$HV = 0.0018544\ (\frac{P}{d^2}) \quad (3)$$

Vickers hardness can also be reported as a unitless number usually described by "HV" followed by the load at which the indent was made e.g. HV30 for Vickers hardness tested at 30 kgf.

In general, the hardness of tungsten carbide cobalt-based metal matrix composites decreases with increasing cobalt content.[1, 4, 87] The Vickers hardness has been reported to be between 15 GPa and 24 GPa for MMCs with 3 to 6 wt. % cobalt decreasing to between 10 to 15 GPa at 15 wt % cobalt and further decreasing to ~8 GPa at 30 wt % cobalt.[1, 4]

2.3.2.2. Transverse rupture strength. Transverse rupture strength (TRS) is the most common strength measurement used to compare amongst MMCs.[1] The TRS of a

material is measured by loading a rectangular specimen across two cylindrical rods and applying a gradually increasing force by means of a third cylindrical rod at the center of the span as outlined in ASTM B406.[1] The TRS of the material is then calculated using Equation 4

$$\sigma = 3PL/2bh^2 \quad (4)$$

where σ is the TRS in MPa, P is the load (N) required to fracture, L (mm) is the length of the span, b (mm) is the width of the specimen, and h (mm) is the thickness of the specimen. In general, the TRS of tungsten carbide cobalt-based MMC's increases with increasing cobalt content up to ~20 wt. % cobalt where the contribution of cobalt content to the strength becomes minimal.[1, 4, 6] The typical range of TRS for tungsten carbide cobalt is ~2 GPa at low cobalt content (5 wt. %) to ~3 GPa at high cobalt content (20 wt. %).[1, 4, 6]

2.3.2.3. Elastic modulus. The elastic modulus of metal matrix composites is typically measured by dynamic excitation.[1, 89, 90] This method of determining elastic modulus is outlined in ASTM C1259. In many metal matrix composites the elastic modulus decreases with increasing metal content due to the modulus of the metal phase being generally lower than that of the ceramic phase.[1, 75] This relationship between elastic modulus and metal content has been explored more thoroughly for tungsten carbide cobalt. Hashin et al. derived a predictive model for the elastic modulus of tungsten carbide cobalt with increasing cobalt content.[91] More recently, Koopman et al. used the upper and lower Hashin-Shtrikman bounds to confirm their dynamic elastic modulus measurements.[90] The results of this study are shown in Figure 2.9.

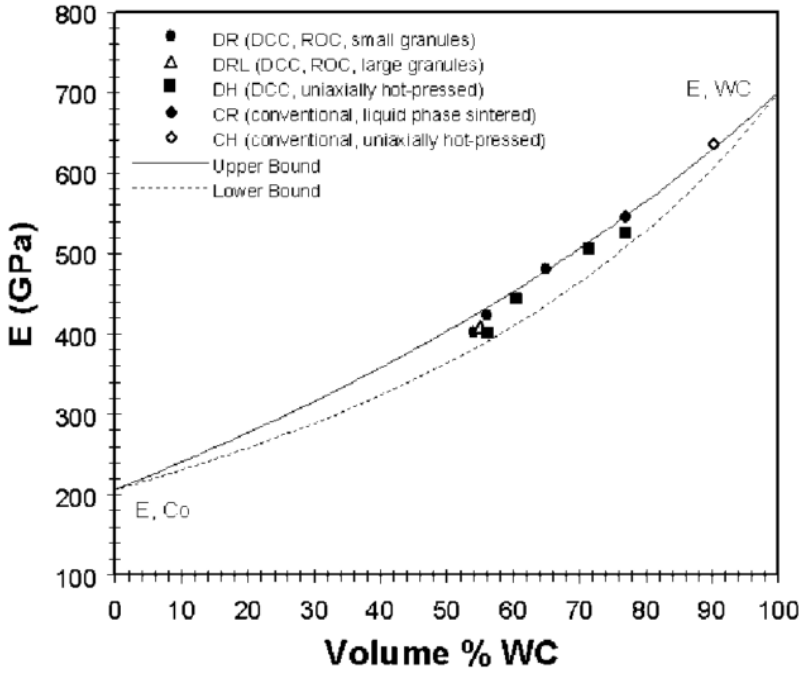

Figure 2.9. Hashin – Shtrikman bounds for Young's modulus and impulse excitation data for the tungsten carbide cobalt system. Taken from Koopman et al..[90]

2.3.2.4. Wear resistance. There are multiple standard and non-standard tests used in the literature and by industry to measure the wear resistance of metal matrix composites.[1, 12, 79, 92] For the purposes of this study this section will focus on ASTM G65. This wear testing method holds a rectangular specimen with a standard force against a rubber wheel as a silica abrasive flows over the wheel for a set number of rotations.[93] A schematic of the wear testing apparatus used in this method is shown in Figure 2.10. The wear resistance is then calculated in terms of volume loss over the course of the test.

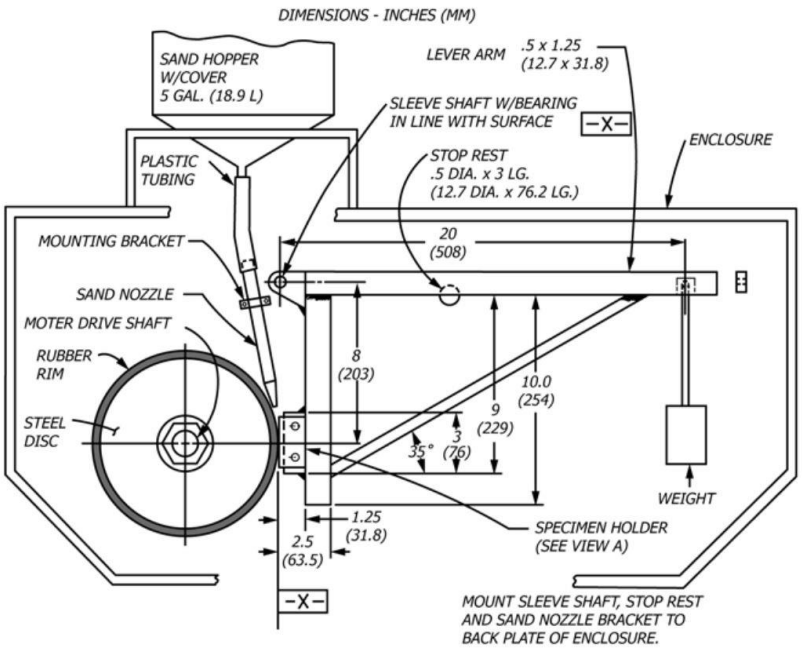

Figure 2.10. Standard wear testing apparatus used in ASTM G65.[93]

The nature of the this and other methods of measuring wear resistance does not allow for much comparison between reported values in the literature and industry. A study by Gant et al. used a modified version of ASTM G65 to test a range of tungsten carbide cobalt MMCs with hardness values between 1000 HV30 and 2000 HV30.[92] The wear volume was reported to be between 1 and 10 mm^3 across the range of tungsten carbide cobalt compositions.[92]

2.3.2.5. Fracture toughness. The fracture toughness of MMCs can be determined by measuring the load needed to break a pre-cracked specimen in four-point bending or by examining the crack propagation from the corners of a Vickers hardness indentation.[1, 47, 94] Another method of testing fracture toughness is chevron notch testing which is outlined in ASTM C1421. The fracture toughness of tungsten carbide cobalt MMCs

increases with increasing cobalt content.[1, 4, 87] The fracture toughness for tungsten carbide 5 wt. % cobalt has been reported to be in the range of 7 – 12 MPa•$m^{1/2}$ increasing to 15 – 25 MPa•$m^{1/2}$ at 25 wt % cobalt.[1, 4, 6]

2.4. TUNGSTEN CARBIDE WITH CU-NI-MN-ZN

The main focus of this study has been to classify a baseline of the tungsten carbide Cu-Ni-Mn-Zn system and improve upon it with the addition of other hard ceramic additives. As previously discussed, much of the information on Cu-Ni-Mn-Zn and its use in brazes and MMCs is contained in trade secrets and patent law.[57, 59, 60] However, Hong et al. has conducted a study on the hardness and wear resistance of tungsten carbide Cu-Ni-Mn-Zn with and without an addition of indium. This study also utilized a pressureless infiltration technique similar to the one used in Paper II in order to produce dense specimens. The study reported that the hardness of tungsten carbide Cu-Ni-Mn-Zn was 108 HRB (aprox. 3 GPa) and a volume loss of 7 mm^3 after 3000 m of a pin-on-disk test at 10 N applied load.[12]

PAPER

I. THE WETTING OF TaC, B_4C, WC, AND SiC BY Cu-Ni-Mn AND Cu-Ni-Mn-Zn ALLOYS

Paul M. Brune*, Jeremy L. Watts, and Gregory E. Hilmas

Materials Science and Engineering Department, Missouri University of Science and Technology, Rolla, Missouri 65409

ABSTRACT

The wetting properties of two copper based alloys, Cu-Ni-Mn and Cu-Ni-Mn-Zn, on TaC, WC, B_4C, and SiC ceramic substrates were investigated by the sessile drop method at 1175°C under flowing argon. The equilibrium contact angles for Cu-Ni-Mn were measured to be 47°, 13°, 0°, and 121° for TaC, B_4C, WC, and SiC, respectively. The equilibrium contact angles for Cu-Ni-Mn-Zn were measured to be 24°, 8°, 0°, and 109° for TaC, B_4C, WC, and SiC, respectively. The metal-ceramic interfaces were examined in cross-section by scanning electron microscopy (SEM), energy dispersive X-ray spectroscopy (EDS), and Raman spectroscopy. It was determined that WC and TaC had a nonreactive interface with the wetting alloys. However, the interface between both alloys and B_4C showed signs of a reaction that produced graphitic carbon at the interface. Similarly, there was an interfacial reaction between SiC and Cu-Ni-Mn that also produced graphitic carbon at the interface.

1. INTRODUCTION

Metal matrix composites (MMCs) are composites that consist of a metal matrix with ceramic reinforcement of some type (e.g. powder or fiber reinforcement). MMCs are made to take advantage of the hardness of the ceramic phase and the toughness of the metal phase in order to produce a composite with both attributes.[1] Copper based MMCs have applications in the nuclear, abrasive, and tooling industires.[2, 3, 4, 5] This is in part due to the excellent wetting of between copper alloys and tungsten carbide allowing for the processing of MMCs by pressureless infiltration.[3, 6]

The contact angle between a liquid and a solid can be defined by Young's equation

$$\gamma_{sv} - \gamma_{sl} = \gamma_{lv}\cos(\theta) \quad (1)$$

where γ_{sv}, γ_{sl}, and γ_{lv} are the surface energies between the solid-vapor, solid-liquid, and liquid-vapor phases and θ is the contact angle between the liquid and the solid.[7] Young's equation is valid for the equilibrium contact angle between a solid and a liquid but does not take into account the kinetics of the formation of the interface or any reactions. This contact angle can be used as a measure of the degree of wetting between a liquid and a solid. Wettability can be measured by a number of techniques, including sessile drop, thin film stability, and resistive film breakthrough pressure experiments.[8,9,10,11] The sessile drop method has been used to determine the contact angle and thus the wettability of a liquid metal on a ceramic substrate. The application of this technique for liquid metals on ceramic substrates is common in the technical literature.[10, 12, 13, 14, 15] In the sessile drop technique a drop of liquid metal falls onto the surface of a solid ceramic

substrate at a set temperature. The drop is observed until the contact angle reaches equilibrium or near equilibrium and the angle is then measured geometrically. Figure 1 shows a schematic of a typical cross section of a liquid-solid contact angle that would be measured in a sessile drop experiment.

The wettability of a metal on a ceramic can also be used as an indicator of its ability to infiltrate into a powder compact of the same ceramic. A contact angle of 90° or less is typically characterized as a wetting relationship since the energy of the system can be reduced by the spreading of the metal, thus creating more interface. However, according to Kaptay et al., the threshold contact angle for spontaneous infiltration is between 70° and 80°.[16] While Young's equation predicts infiltration below a threshold of 90°, this does not account for the complex geometry of the pore network inside a powder compact. The equations used by Kaptay et al. account for this complex geometry. Thus, for the production of metal matrix composites via spontaneous infiltration, the equilibrium contact angle would have to be lower than at least 70° and ideally as low as 0° at the processing temperature.

The wetting properties of two copper based alloys, Cu-Ni-Mn and Cu-Ni-Mn-Zn, were evaluated for TaC, B_4C, WC, and SiC ceramic substrates in order to determine their viability for the production of metal matrix composites via spontaneous infiltration. This has been accomplished through the use of sessile drop experiments at a typical processing temperature of 1175°C under flowing argon. The interfaces were then examined to determine what if any reaction took place at the interface.

2. PROCEDURE

2.1. Specimen Preparation

Four different ceramic substrates were used for targets in sessile drop experiments. The SiC substrate (Trex Enterprises Corperation, Lihue, HI) was fabricated using plasma enhanced chemical vapor deposition. The WC substrate was nominally pure, binderless material (RC500, Kennametal, Latrobe, PA). The B_4C substrate was produced by hot pressing B_4C to near theoretical density (99.6%). The TaC substrate was produced by hot pressing (HP20-3060-20,Thermal Technology, Santa Rosa, CA) TaC powder (TA-301, Atlantic Equipment Engineers, Bergenfield, NJ) with a 0.36 wt. % addition of B_4C powder (HS grade, H.C. Starck, Newton, MA) to aid in sintering in a 1 inch diameter graphite die (Graphite Products Corp, Madison Heights, MI) coated in boron nitride (Cerac, SP-108, Milwaukee, WI) at 2200°C and 30 MPa in helium atmosphere according to Zhang et al..[17] All substrates were cut into 25 mm squares with a resin bonded diamond cutting wheel using a surface grinder (FSG-3A818, Chevalier, Santa Fe Springs, CA). The various substrates were then prepared by polishing with sequentially finer resin-bonded diamond pads from 45 μm to 3 μm then with sequentially finer diamond abrasive slurries (South Bay Technologies, San Clemente, CA) from 3 μm to 0.25 μm. Copper-nickel-manganese and copper-nickel-manganese-zinc alloys were sectioned into 0.2 gram slices with a diamond wafering saw (VC50, Leco, Saint Joseph, MI) to produce uniform quantities for sessile drops.

2.2. Experimental

The sessile drop experiments were performed under flowing argon in an alumina tube furnace (1730-20HTF, CM Furnaces, Bloomfield, NJ). The substrate was placed

into an alumina holder under a graphite stand. Graphite was used for the parts that would come into contact with the metal because the metal does not wet it. The graphite stand had a funnel machined in its center where the binder metal was placed. The experimental setup is shown in cross section in Figure 2. The temperature was then ramped at 10°C/min to 1175°C and held for 1 hour. The temperature at which the metal droplet would fall from the graphite stand was controlled by the melting temperature of the alloy being used. The experiment was recorded on a digital camera (DXC HX400V, Sony, Tokyo, Japan) from the outside of the furnace with a view of the side profile of the sessile drops in situ. Stop-frame images were taken from the recordings and were used to measure the contact angle as a function of time and temperature. These measurements were obtained by measuring the angle between the drop and substrate using computerized image analysis (ImageJ, National Institutes of Health, Bethesda, MD).

2.3. Analysis

Drop/substrate cross sections were prepared for analysis using the sectioning and polishing methods described above. The metal-ceramic interfaces were then examined using optical microscopy (KH-8700, Hirox, Hackensack, NJ), scanning electron microscopy (SEM) (S-4700, Hitachi, Tokyo, Japan) (Helios Nanolab 600, FEI, Hillsboro, OR), energy dispersive X-ray spectroscopy (EDS), and Raman spectroscopy (Aramis Labram, Horiba Jobin Yvon, Edison, NJ).

3. RESULTS AND DISCUSSION

3.1. Tantalum Carbide and Tungsten Carbide

The contact angles of each binder metal, recorded upon initial contact with the ceramic substrate and after one hour at 1175°C, are shown in Table 1. For both TaC and

WC the contact angle of the Cu-Ni-Mn and Cu-Ni-Mn-Zn metals decreased with increasing temperature. The intial contact angles on TaC were 93° for Cu-Ni-Mn and 104° for Cu-Ni-Mn-Zn. The final contact angle on TaC was 47° for Cu-Ni-Mn and 24° for Cu-Ni-Mn-Zn. While the initial contact angles for Cu-Ni-Mn and Cu-Ni-Mn-Zn on TaC were greater than 70°, which is required for spontaneous infiltration, both final angles were well below that threshold. WC had the lowest contact angles of all the carbides tested for both metals. The initial contact angle of Cu-Ni-Mn on WC was 30° and the final contact angle was 0°, which means that the metal fully spread across the surface of the WC substrate. The Cu-Ni-Mn-Zn metal has an initial contact angle of 0° on WC and the metal continued to spread across the surface throughout the experiment.

The cross sections of the metal-ceramic interfaces were examined to determine if there were reactions at the interface. Figure 3 shows an SEM micrograph of the interface between the TaC substrate and Cu-Ni-Mn metal. The interface shows no evidence of pitting or secondary compound formation. Similarly, the interface between TaC and Cu-Ni-Mn-Zn did not show any evidence of a reaction. The interface between the Cu-Ni-Mn-Zn metal and the WC substrate was examined by optical microscopy in Figure 4. The interface is similar in that there is no evidence of a reaction occurring between the WC and the Cu-Ni-Mn-Zn metal. The interface between WC and Cu-Ni-Mn-Zn also did not show evidence of interfacial reactions.

3.2. Boron Carbide

From Table 1, the initial contact angle on B_4C was 56° for Cu-Ni-Mn and 114° for Cu-Ni-Mn-Zn. The final contact angle on B_4C was 13° for Cu-Ni-Mn and 8° for Cu-Ni-

Mn-Zn. As with WC and TaC, the contact angles between both metals and B_4C decreased as a function of time and temperature during the sessile drop experiments. While the initial contact angle between Cu-Ni-Mn-Zn and B_4C was higher than the threshold for spontaneous infiltration, the final contact angle was well below 90°.

A SEM micrograph of the cross section of the B_4C substrate and Cu-Ni-Mn-Zn metal droplet is shown in Figure 5. The interface between the two is marked by a reaction layer between the alloy and the substrate. There is also evidence of segregation in the Cu-Ni-Mn-Zn metal. The dark phase in the reaction layer on the interface was determined to be graphitic carbon by Raman spectroscopy. The graph in Figure 6 shows the Raman spectra for the dark phase with a peak at 1341 cm^{-1} and a peak at 1595 cm^{-1} which is similar to known spectra for graphite in the literature.[18, 19, 20] These two peaks correspond to the D-band which is found at ~ 1355 cm^{-1} and the G-band found at ~1575 cm^{-1}.[21] The D-band peak is associated with in-plane vibrations and results from disorder in the graphite structure.[18] The G-band peak is the characteristic peak in graphite and can shift to ~1600 cm^{-1} in disordered graphite.[18] EDS was used to determine how the alloy segregated around the interface. An EDS map for the cross section between B_4C and Cu-Ni-Mn-Zn is shown for Cu, Ni, and Mn in Figure 7. From the EDS maps it can be concluded that the Cu and Mn separated in bands parallel to the interface. The boron could not be reliably identified in the microstructure by the EDS used in this study due to limitations in its capability to distinguish between light elements. The evidence of graphite at the interface, and the separation of the alloy, could be evidence of the dissociation of B_4C into boron and graphitic carbon. A similar reaction was proposed by Froumin et al. between pure copper and B_4C at 1200°C. The study further concluded that

boron had dissolved into liquid solution at temperature and precipitated at the copper grain boundaries upon solidification.[22] While boron could not be identified in the binder metal, it is possible that the manganese could have reacted with boron to form a boride. This is supported by the existence of metal borides in the B-Mn phase diagram.[23] Another study observed that carbon at the reaction interface of copper alloys and B_4C could inhibit further wetting in applications such as infiltration.[24]

3.3. Silicon Carbide

The contact angle between Cu-Ni-Mn and SiC was initially 121°C and did not change over time, unlike all the other metal-substrate contact angles in this experiment. The initial contact angle between Cu-Ni-Mn-Zn and SiC was 85°. The contact angle increased over the course of the experiment to a final contact angle of 109°. Neither of the final contact angles fell below the 70° threshold for infiltration. The interface between SiC and Cu-Ni-Mn was examined by optical microscopy, SEM, and EDS. Figure 8A shows the cross section of the alloy drop on SiC. From the optical image, it is clear that there is a reaction at the interface as well as separation in the alloy. Figure 8B shows the microstructure of the reaction layer between the Cu-Ni-Mn metal and SiC in the area shown in the box on Figure 8A. EDS analysis of the region depicted in Figure 8B confirmed that the dark phase is carbon and that the light phase is a mix of Cu and Ni-Mn-Si metal. The separation of SiC into silicon and carbon upon reacting with copper has been reported in literature.[25, 26, 27, 28] The proposed reaction by Liu et al. for both copper and nickel is expressed as Equation 2.

$$\mathrm{Me} + \mathrm{SiC} \rightarrow \mathrm{Silicide} + \mathrm{C} \qquad (2)[28]$$

It is hypothesized that the SiC decomposed into silicon and carbon upon contact with the alloy droplet resulting in a volume change in the substrate at the interface. The silicon metal then dissolved into the alloy and the alloy infiltrated into the open volume. This hypothesis is supported by observations by Shimbo et al. with Cu sessile drops on SiC. In these experiments, it was observed that Cu metal would decompose SiC and dissolve into the ceramic.[26] Figure 9 shows the interface between the unreacted SiC and Cu-Ni-Mn metal at the bottom of the reaction layer. As with B_4C, the presence of carbon at the interface will inhibit wetting and lead to incomplete spontaneous infiltration. The wetting issue can however be remedied as Zhan et al. has shown improvement in the infiltration behavior of copper and SiC by coating the SiC particles with nickel before infiltrating.[29] Additions of silicon to the binder metal may reduce the amount of carbon at the interface by inhibiting the dissociation of SiC; just as the additions of boron to the binder metal inhibited the dissociation of B_4C as shown by Froumin et al. Unfortunately, the Cu-Ni-Mn-Zn alloy droplets did not adhere to the SiC substrates during cooling and could not be reliably examined in cross-section.

4. SUMMARY

The wetting properties of two copper based alloys, Cu-Ni-Mn and Cu-Ni-Mn-Zn, were determined for TaC, WC, B_4C, and SiC by the sessile drop method. It was determined that, overall, the Cu-Ni-Mn alloy had a higher contact angle than the Cu-Ni-Mn-Zn alloy on SiC, B_4C and TaC. Additionally, it was shown that TaC, WC, and B_4C were wet by both alloys while SiC was not wet by either alloy at 1175°C. However, carbon formation at the interfaces of B_4C and SiC with both metal alloys may inhibit infiltration. The interface between Cu-Ni-Mn and SiC was examined by SEM and EDS

and it was shown that SiC reacted with the alloy to form carbon at the interface and may have dissolved silicon into the metal alloy. There is also evidence that this alloy may have infiltrated into the carbon rich reaction layer. Both WC and TaC show favorable interfacial properties with final contact angles of 47° and 0° respectively for Cu-Ni-Mn and final contact angles of 24° and 0° respectively for Cu-Ni-Mn-Zn. These contact angles are lower than 70°, making them viable candidates for spontaneous infiltration.

FIGURES AND TABLES

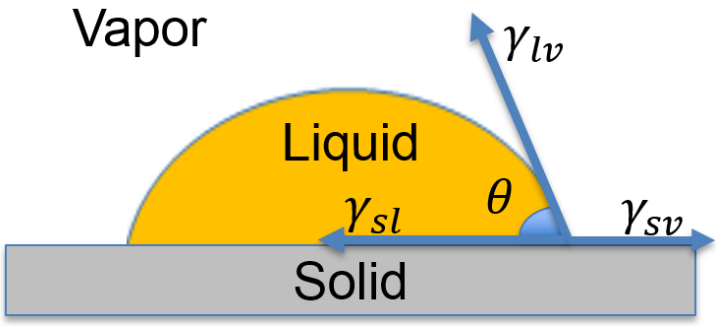

Figure 1. Equilibrium contact angle of a liquid on a solid substrate in cross section.

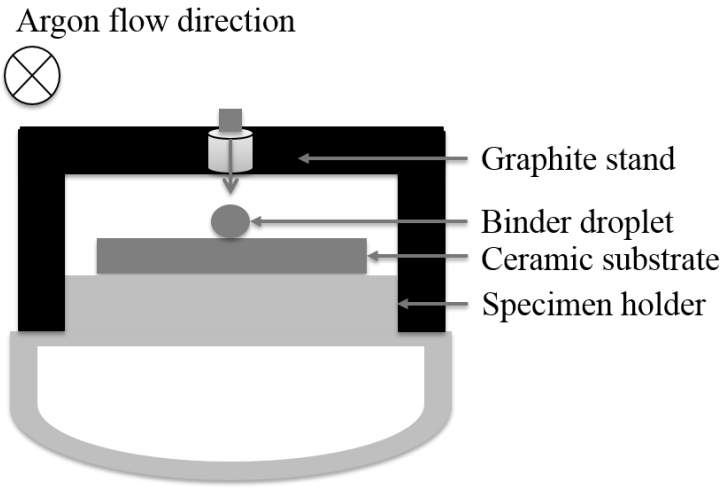

Figure 2. Cross section of sessile drop experimental setup.

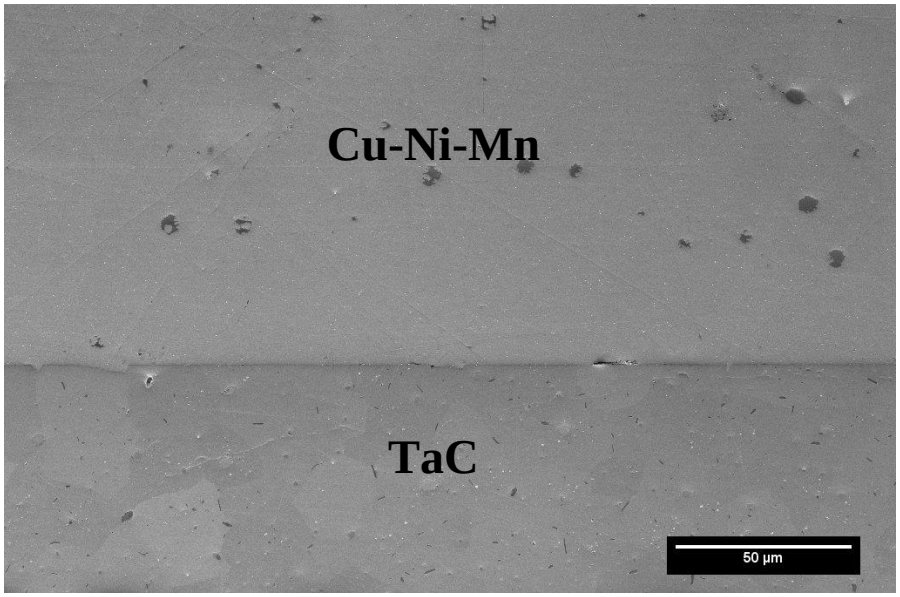

Figure 3. SEM micrograph of the interface between Cu-Ni-Mn alloy (top) and TaC substrate (bottom).

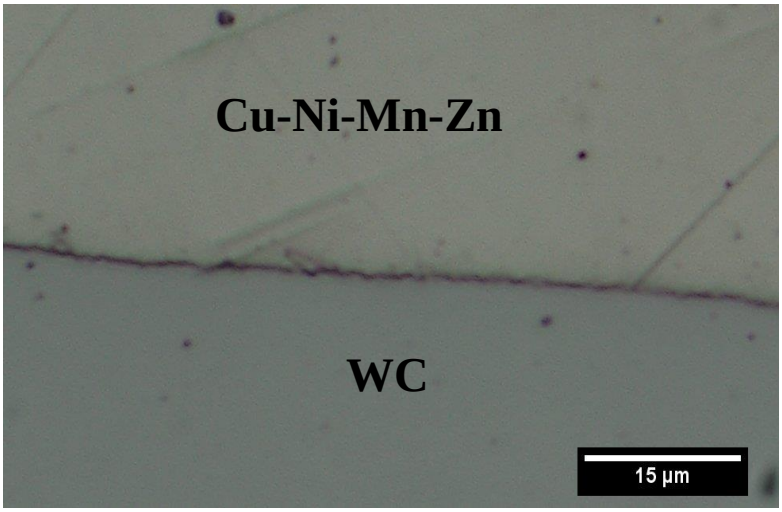

Figure 4. Optical micrograph of the interface between Cu-Ni-Mn alloy (top) and WC substrate (bottom).

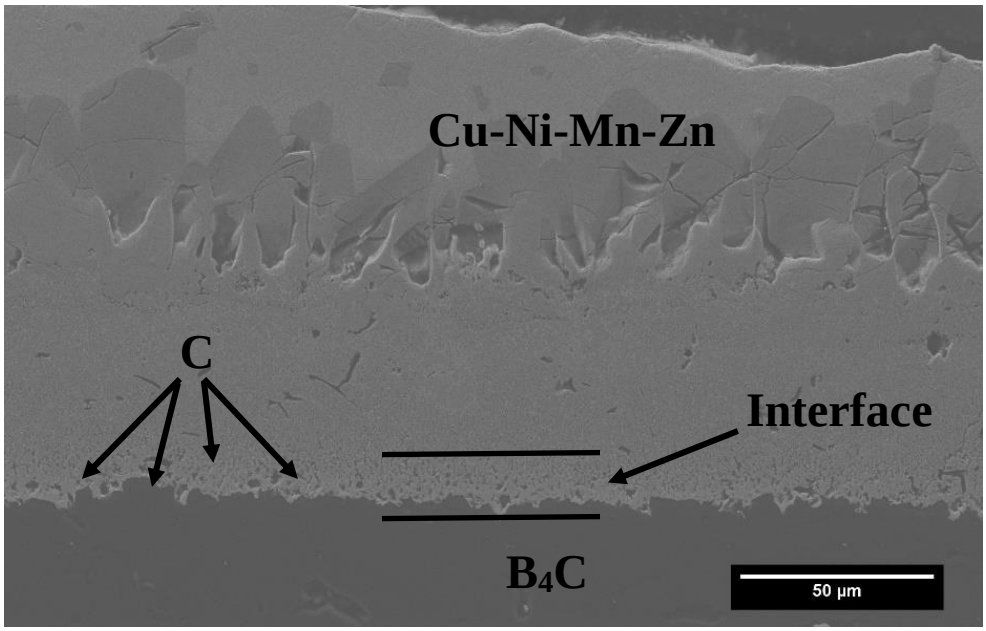

Figure 5. SEM micrograph of the interface between the Cu-Ni-Mn-Zn alloy (top) and the B_4C substrate (bottom). The interface has been shown to contain carbon.

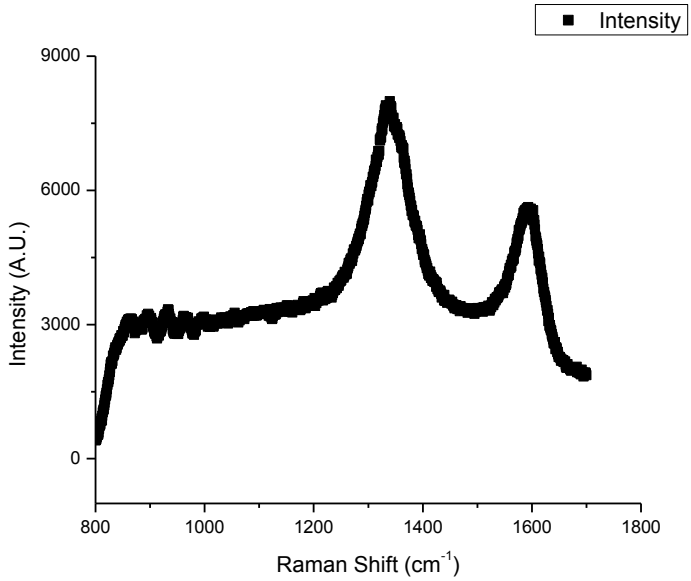

Figure 6. Raman spectra for the dark phase in B4C/Cu-Ni-Mn-Zn interface.

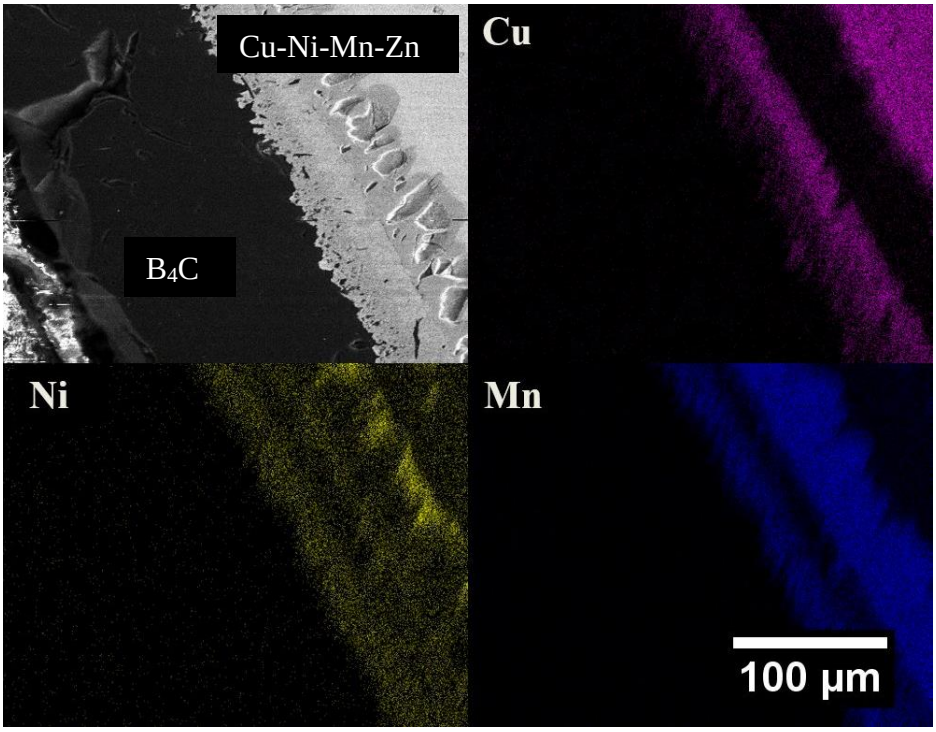

Figure 7. EDS map of the cross-sectional interface of Cu-Ni-Mn-Zn on B_4C.

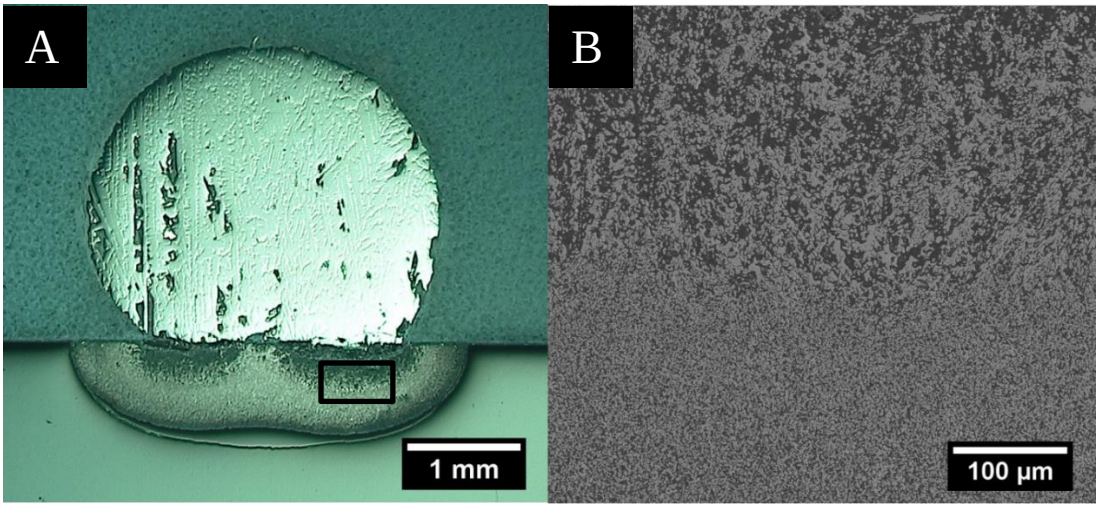

Figure 8. (A) Cu-Ni-Mn alloy droplet on SiC with reaction layer at interface and cooling crack below. (B) SEM micrograph of reaction interface in the area designated by the box from Figure 9A.

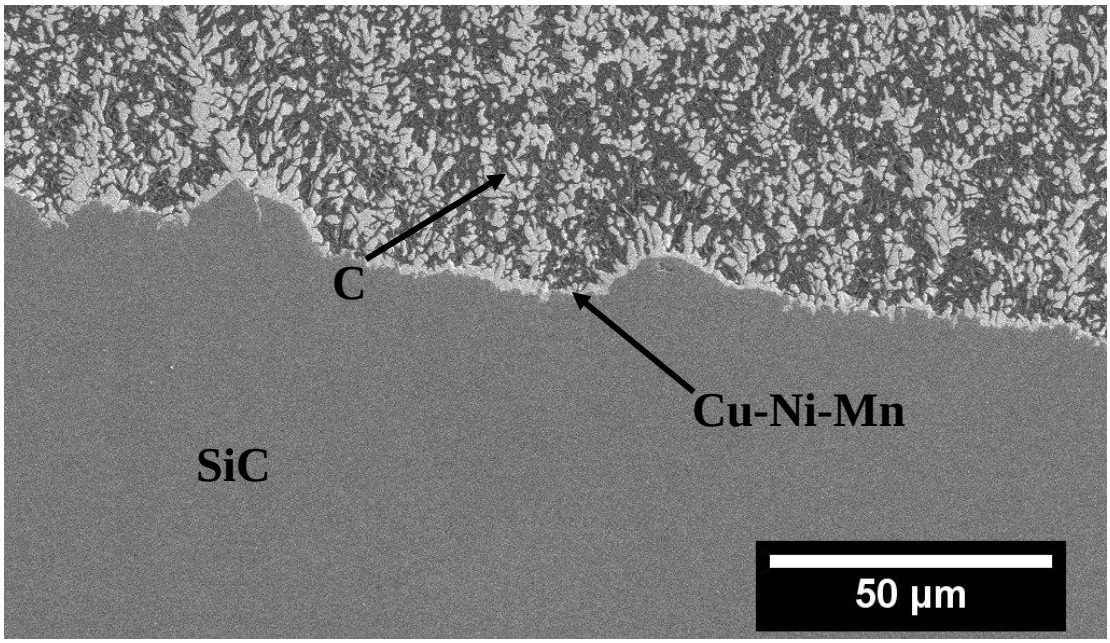

Figure 9. The bottom of the reaction layer between Cu-Ni-Mn and SiC. The SiC appears to be coated in metal (light phase).

Table 1. Contact angles for Cu-Ni-Mn and Cu-Ni-Mn-Zn on various substrates at initial contact with the substrate and after one hour at 1175°C.

Substrate	Cu-Ni-Mn		Cu-Ni-Mn-Zn	
	Initial (~1150°C)	Final (1175°C)	Initial (~1000°C)	Final (1175°C)
TaC	93°	47°	104°	24°
WC	30°	0°	0°	0°
B_4C	56°	13°	114°	8°
SiC	121°	121°	85°	109°

REFERENCES

1. G. S. Upadhyaya, "Materials science of cemented carbides — an overview," *Materials & Design,* 22[6] 483-89 (2001).

2. T. Maruyama and S. Onose, "Fabrication and Thermal Conductivity of Boron Carbide/Copper Cermet," *J. Nucl. Sci. Technol.*, 36[4] 380-85 (1999).

3. E. Hong, B. Kaplin, T. You, M.-s. Suh, Y.-S. Kim, and H. Choe, "Tribological properties of copper alloy-based composites reinforced with tungsten carbide particles," *Wear*, 270[9–10] 591-97 (2011).

4. J. Liu, S. Yang, K. Liu, C. Gui, and W. Xia, "Effect of Age-Hardening Treatment on Microstructure and Sliding Wear-Resistance Performance of WC/Cu-Ni-Mn Composite Coatings," *MMTA,* 48[6] 3017-26 (2017).

5. P. K. Deshpande and R. Y. Lin, "Wear resistance of WC particle reinforced copper matrix composites and the effect of porosity," *Materials Science and Engineering: A,* 418[1–2] 137-45 (2006).

6. P. K. Deshpande, J. H. Li, and R. Y. Lin, "Infrared processed Cu composites reinforced with WC particles," *Materials Science and Engineering: A,* 429[1–2] 58-65 (2006).

7. T. Young, "An Essay on the Cohesion of Fluids," *Philos. Trans. R. Soc. London,* 95 65-87 (1805).

8. R. K. Everett, "Metal Matrix Composites: Processing and Interfaces (Treatise on Materials Science and Technology)," pp. 228. Academic Press: 1250 Sixth Avenue. San Diego, CA, (1991).

9. W. D. Kingery and M. Humenik, "Surface Tension at Elevated Temperatures. I. Furnace and Method for Use of the Sessile Drop Method; Surface Tension of Silicon, Iron and Nickel," *The Journal of Physical Chemistry,* 57[3] 359-63 (1953).

10. M. Humenik and W. D. Kingery, "Metal-Ceramic Interactions: III, Surface Tension and Wettability of Metal-Ceramic Systems," *J. Am. Ceram. Soc.,* 37[1] 18-23 (1954).

11. W. D. Kingery, "Metal-Ceramic Interactions:IV, Absolute Measurement of Metal-Ceramic Interfacial Energy and the Interfacial Adsorption of Silicon from Iron-Silicon Alloys," *J. Am. Ceram. Soc.,* 37[2] 42-45 (1954).

12. F. Delannay, L. Froyen, and A. Deruyttere, "The wetting of solids by molten metals and its relation to the preparation of metal-matrix composites composites," *Journal of Materials Science,* 22[1] 1-16 (1987).

13. R. Sangiorgi, G. Caracciolo, and A. Passerone, "Factors limiting the accuracy of measurements of surface tension by the sessile drop method," *Journal of Materials Science,* 17[10] 2895-901 (1982).

14. G. V. Samsonov, A. D. Panasyuk, and G. K. Kozina, "Wetting of refractory carbides with liquid metals," *Soviet Powder Metallurgy and Metal Ceramics,* 7[11] 874-78 (1968).

15. I. A. Aksay, C. E. Hoge, and J. A. Pask, "Wetting under chemical equilibrium and nonequilibrium conditions," *The Journal of Physical Chemistry,* 78[12] 1178-83 (1974).

16. G. Kaptay and T. BÁrczy, "On the asymmetrical dependence of the threshold pressure of infiltration on the wettability of the porous solid by the infiltrating liquid," *Journal of Materials Science,* 40[9-10] 2531-35 (2005).

17. X. Zhang, G. E. Hilmas, W. G. Fahrenholtz, and D. M. Deason, "Hot Pressing of Tantalum Carbide With and Without Sintering Additives," *J. Am. Ceram. Soc.,* 90[2] 393-401 (2007).

18. H. Feng, X. Wang, and D. Wu, "Fabrication of Spirocyclic Phosphazene Epoxy-Based Nanocomposites with Graphene via Exfoliation of Graphite Platelets and Thermal Curing for Enhancement of Mechanical and Conductive Properties," *Industrial & Engineering Chemistry Research,* 52[30] 10160-71 (2013).

19. A. C. Ferrari, J. C. Meyer, V. Scardaci, C. Casiraghi, M. Lazzeri, F. Mauri, S. Piscanec, D. Jiang, K. S. Novoselov, S. Roth, and A. K. Geim, "Raman Spectrum of Graphene and Graphene Layers," *Phys. Rev. Lett.,* 97[18] 187401 (2006).

20. R. Vidano and D. B. Fischbach, "New Lines in the Raman Spectra of Carbons and Graphite," *J. Am. Ceram. Soc.,* 61[1-2] 13-17 (1978).

21. F. Tuinstra and J. L. Koenig, "Raman Spectrum of Graphite," *The Journal of Chemical Physics,* 53[3] 1126-30 (1970).

22. N. Froumin, N. Frage, M. Aizenshtein, and M. P. Dariel, "Ceramic–metal interaction and wetting phenomena in the B4C/Cu system," *J. Eur. Ceram. Soc.,* 23[15] 2821-28 (2003).

23. B. Predel, "B-Mn (Boron-Manganese)," pp. 1-3. in B-Ba – C-Zr**.** Edited by O. Madelung. Springer Berlin Heidelberg, Berlin, Heidelberg, 1992.

24. S. Tariolle, F. Thévenot, M. Aizenstein, M. P. Dariel, N. Frumin, and N. Frage, "Boron carbide–copper infiltrated cermets," *J. Solid State Chem.,* 177[2] 400-06 (2004).

25. C. Rado, B. Drevet, and N. Eustathopoulos, "The role of compound formation in reactive wetting: the Cu/SiC system," *Acta Mater.,* 48[18–19] 4483-91 (2000).

26. 26. M. Shimbo, M. Naka, and I. Okamoto, "Wettability of silicon carbide by aluminium, copper and silver," *J. Mater. Sci. Lett.*, 8[6] 663-66 (1989).

27. T. Köck, A. Brendel, and H. Bolt, "Interface reactions between silicon carbide and interlayers in silicon carbide–copper metal–matrix composites," *J. Nucl. Mater.*, 362[2–3] 197-201 (2007).

28. G. W. Liu, M. L. Muolo, F. Valenza, and A. Passerone, "Survey on wetting of SiC by molten metals," *Ceram. Int.*, 36[4] 1177-88 (2010).

29. Y. Zhan and G. Zhang, "The effect of interfacial modifying on the mechanical and wear properties of SiCp/Cu composites," *Mater. Lett.*, 57[29] 4583-91 (2003).

II. THE PROCESSING AND PROPERTIES OF WC-BASED/Cu-Ni-Mn-Zn METAL MATRIX COMPOSITES

Paul M. Brune*, Jeremy L. Watts, and Gregory E. Hilmas

Materials Science and Engineering Department, Missouri University of Science and Technology, Rolla, Missouri 65409

ABSTRACT

Various WC/Cu-alloy based metal matrix composites (MMCs) were produced using a pressureless infiltration technique. The effects of 10 vol% substitutions of VC, cBN, and TaC on the microstructure and mechanical properties were investigated. The VC containing MMCs were observed to have areas of pullout in part due to the embrittlement of the WC caused by VC. Additionally, it was found that cBN did not form a strong chemical bond with the matrix resulting in agglomeration and pockets of porosity. The TaC containing composites had agglomeration of smaller TaC particles ranging from 3 to 10 μm. This agglomeration was partially infiltrated in the MTaC3 composition, but unlike in the cBN containing composition the TaC particles formed a chemical bond with the metal matrix. The composition containing 10% TaC outperformed the baseline composition in transverse rupture strength with a TRS of 1000 ± 47 MPa vs 838 ± 61 MPa. It was also shown that the substitution of TaC improved the fracture toughness over the baseline composition by around 3-6 MPa•$m^{1/2}$. However, there was no appreciable change in wear resistance due to the addition of TaC into the microstructure.

1. INTRODUCTION

Tungsten carbide based metal matrix composites (MMC) are prevalent in many areas of the automotive, machining, and mining industries due to the hardness imparted by the ceramic particulate and the toughness of the metal binder phase.[1, 2, 3] For decades, WC-Co based metal matrix composites have saturated the market. However, there has been research into other substitutes for cobalt in the literature including iron[4], nickel[1, 4] and copper[5, 6, 7]. The current focus of this research is on a Cu-based alloy of Cu-Ni-Mn-Zn. This alloy has been noted to have excellent wetting characteristics in relation to WC, and wear resistance.[8]

Additionally, there has been considerable research into reinforcing phases in addition to tungsten carbide for WC-based MMCs. Tantalum carbide, vanadium carbide, niobium carbide, and chromium carbide are all common additives in these MMCs, added to inhibit grain growth and improve mechanical properties.[2, 4] While the effects of these additives have been explored in other metal matrix composites, there is little in the current body of research for WC/Cu-Ni-Mn-Zn.

The focus of this research will be to explore the effects of TaC, VC, and cBN on the microstructure, transverse rupture strength, fracture toughness, and wear resistance of WC-based MMCs with the goal of improving one or more of the aforementioned mechanical properties without adversely affecting the others. MMCs used in this study were prepared using pressureless infiltration as opposed to other methods common to WC-Co composites. This technique has been shown in the literature to be a viable method of producing the base WC MMC used in this study.[8]

2. PROCEDURE

2.1. Processing

Tungsten carbide, two types of tantalum carbide, boron carbide, vanadium carbide, and cubic boron nitride powders were obtained as outlined in Table 1. These powders were batched into various compositions that include a baseline 100 vol% tungsten carbide powder and compositions of 90 vol% tungsten carbide powder and 10 vol% of another carbide or nitride powder, as listed in Table 1. These compositions were mixed by ball milling in acetone with 7/32 inch tungsten carbide cobalt milling media at 30 rpm for one hour. The powders were then dried by rotary evaporation (Roto-vapor R-124; Buchi, Flawil, Switzerland) at a temperature of 80°C, vacuum of 68 kPa and a rotation speed of 75 rpm. Dried powders were then sieved with a 60 mesh screen to break up soft agglomerates. The powders were then poured into a graphite mold and settled on a vibratory table to achieve a uniform pack density. Cubes of a Cu-Ni-Mn-Zn binder alloy were then placed on a graphite sieve in the upper portion of the mold suspended above the powder bed. A schematic of this process is shown in Figure 1. Infiltration was achieved by use of a bottom-fed box furnace (DT 31-9, Deltech Inc., Denver, CO) at 1175°C under argon flow. Below 1175°C the furnace was heated at a rate of 10°C/min. Once at temperature, the furnace bed was lowered and the graphite mold was inserted. The furnace was allowed to recover to 1175°C and then the mold was held at temperature for 10 to 50 minutes depending on composition as outlined in Table 2. The mold was then taken out of the furnace and cooled freely in air to room temperature. The puck of metal matrix composite was then machined into various samples for microstructural characterization and mechanical testing.

2.2. Characterization

Specimens used in microstructural characterization were machined by sectioning the puck parallel to the infiltration direction using electronic discharge machining (EDM: AgieCut HSS150, GF Manufacturing Technology, Switzerland). The specimens were then ground flat on a surface grinder (FSG-3A818; Chevalier, Santa Fe Springs, CA) with a 600-grit resin-bonded diamond wheel. The samples were then ground and polished to a 0.25 μm surface finish using successively finer diamond abrasive slurries (South Bay Technologies, San Clemente, CA). Scanning electron microscopy (SEM; S4700, Hitachi, Japan and Helios Nanolab 600, FEI, Hillsboro, OR) was used to obtain micrographs of each of the compositions. Secondary phases were characterized by use of energy dispersive X-ray spectroscopy (EDS) and X-ray diffraction (XRD; X'Pert Pro, PANalytical, Almelo, Netherlands) . Area fractions of phases were determined by examining at least 200,000 μm^2 per composition with image analysis software (ImageJ, National Institutes of Health, Bethesda, MD).

2.3. Mechanical Properties

Specimens were cut parallel to the infiltration direction as previously stated. Transverse rupture strength (TRS) bars were machined by grinding with a 400-grit resin bonded diamond wheel perpendicular to the testing direction. The bars were ground to 0.25 in x 0.20 in ± 0.01 in as per ASTM B406.[9] The as ground surfaces were sand blasted with 120 grit aluminum oxide media before being tested in bending using an instrumented load frame (5881, Instron, Norwood, MA).

Hardness testing was performed on specimens of each composition and prepared in the same manner as specimens used to obtain SEM micrographs. Vickers hardness

indentations (Duramin 5, Leco, St. Joseph, MI) were performed in accordance with ASTM C1327 at 50 kgf to ensure a large enough indentation for a representative measurement.[10]

Specimens for fracture toughness testing were cut, perpendicular to the infiltration direction, as bars measuring at least 3 mm x 4 mm x 44 mm by EDM. The bars were then ground flat and parallel using a 120 grit resin-bonded diamond wheel on a surface grinder. A chevron, as defined by ASTM C1421, was then machined into the tensile surface of the bars using a pneumatic saw (Accu-cut 5200, Aremco Products, Ossining, NY).[11] The bars were then tested in bending using an instrumented load frame (Instron 5881, Instron, Norwood, MA).

Specimens for wear testing were cut as plates of at least 25.4 mm x 25.4 mm x 6.4 mm parallel to the infiltration direction. and ground with a 600-grit resin bonded diamond wheel on a surface grinder on the surface to be tested. This was to ensure that the testing surfaces would sit flat and parallel in the wear testing apparatus. The testing apparatus[12] was prepared as outlined in ASTM G65 and the specimens were tested according to procedure A, 6000 revolutions of a 9 inch wheel.[13]

3. RESULTS AND DISCUSSION

3.1. Microstructure

The microstructures of the various composites were examined using SEM and ImageJ analysis. Figure 2 shows the typical microstructure for the baseline WC based MMC. Some spherical porosity and pockets of matrix material are prevalent in the microstructure. The area fractions of particulate, porosity, and binder content were

measured and are listed in Table 3. From Table 3 the binder area fraction for McBN is 0.54, which is 0.10 higher than the baseline composition and the highest measured of all compositions. Since the density of cBN is 3.45 g/cm^3,[14] which is lower than that of WC, it may have interacted differently during infiltration than TaC and VC. One possibility is that the cBN floated to the top of the puck, leaving room for more metal to infiltrate into the powder compact. A study by Shao et al. showed that cBN was buoyant in a Ni based alloy when the powders were loosely packed.[15] The porosity of the McBN composition was measured to be 0.10 compared to the baseline composition with a porosity of 0.01. This difference was likely the result of the agglomeration of the cBN powder in the microstructure along with non-reactivity between the binder metal and the cBN powder. Figure 3 shows the typical microstructure of the McBN composite. The typical feature throughout the microstructure is porosity in areas where cBN is present and agglomeration of the cBN particles. Figure 4 shows a close up of a cBN particle surrounded by the Cu-Ni-Mn-Zn matrix. From inspection of the figure, it is probable that the cBN particles are not chemically bonded to the matrix but instead are only mechanically bound.

The MVC composite also had a higher porosity area fraction, 0.03, than the baseline, 0.01, and both TaC compositions, 0.02. From Table 3, the MVC composite is closest to the MTaC3 composite in area fraction of particulate and binder metal. However, the MVC composite differs in that it contains void space, mainly in the form of pulled out WC and VC particles. This is illustrated in Figure 5 where the shape of the porosity in the microstructure closely resembles that of the carbide particles. An EDS analysis, shown in Figure 6, suggests that the VC and WC have gone into solid solution

with one another. This could lead to an embrittlement of the carbide particles which could lead to the pullout shown in Figure 5. This embrittlement has been observed in the literature for WC-Co based MMCs with VC additions.[2]

The microstructures of the MTaC3 and MTaC10 compositions are similar to the baseline microstructure. Figure 7 shows the typical microstructure for the MTaC3 composition. Unfortunately, it was difficult to differentiate TaC and WC in SEM micrographs due to their similar Z contrast. However, TaC has a distinct gold color that can easily be identified under light microscopy. The agglomerates in Figure 7 were confirmed to be composed of TaC in this manner. Many of the TaC agglomerates in the MTaC3 microstructure were unable to be infiltrated. Figure 8 shows the typical microstructure for the MTaC10 composition. The TaC agglomerates were identified in Figure 8 in the same manner as they were identified in the TaC3 microstructure. While there were still TaC agglomerates in the MTaC10 composition, they were successfully infiltrated. The reason for the difference in infiltration behavior is likely related to the size of the TaC powder and the spacing between the particles in the agglomerates. Even with the infiltration problems in the MTaC3 microstructure the measured area fraction of porosity was the same as the MTaC10 composition, 0.02. The MTaC10 composite had the highest area fraction of carbide out of all the compositions including the baseline.

3.2. Mechanical Properties

The hardness, transverse rupture strength (TRS), and fracture toughness of the various composites are given in Table 4. The hardness of the baseline composition was measured to be 3.3 ± 0.2 GPa. In a similar study by Hong et al., WC/Cu-Ni-Mn-Zn composites with 62 vol. % carbide phase were produced by pressureless infiltration. The

hardness of this composition was measured to be 108.4 HRB or ~3 GPa.[8] In a study by Deshpande et al. a WC/Cu composite with 53 vol % WC was indented with a Vickers hardness tester. The hardness was measured to be 3.57 ± 0.15 GPa which is within the standard deviation of the baseline used in this study.[7] Both the TaC containing composites fell within the standard deviation of the baseline composition with an average hardness of 3.3 ± 0.4 GPa for MTaC3 and 3.2 ± 0.2 GPa for the MTaC10 composite. The hardness of the MVC and McBN compositions tested below that of the baseline composition with both the VC and cBN compositions having a hardness of 2.8 ± 0.2 GPa. The hardness of the MVC composite may be a result of the embrittlement of the microstructure as previously discussed. The decrease in hardness for the McBN composition is likely related to the increase in porosity, as shown in Table 3, but could also be related to the high binder area fraction. In general, the hardness of WC/Co decreased with increasing cobalt content.[2, 3, 16] The Vickers hardness of WC/Co composites with 54 vol % Co was reported to be in the range of 7.4 GPa to 7.7 GPa.[17, 18]

The baseline composition had a TRS of 838 ± 61 MPa. In general, the TRS of WC/Co increases with increasing cobalt content up to ~20 wt. % Co where the contribution of Co content to the strength becomes minimal.[2, 3, 17] The Vickers hardness of WC/Co composites with 54 vol % Co was reported to be in the range of 2.8 GPa to 3.3 GPa.[17, 18] The MVC composition had the lowest measured TRS at 743 ± 57 MPa followed by the McBN composition at 806 ± 23 MPa. This trend is similar to the trend seen in the hardness measurements and is likely related to the proposed embrittling effect of VC on WC. The decrease in TRS for the McBN composition is likely caused by the agglomeration of the cBN particles and the way that the cBN interacts with the Cu-Ni-

Mn-Zn matrix. The TRS of the MTaC3 composition was closest to the baseline with a TRS of 847 ± 36 MPa while the MTaC10 measured higher with a TRS of 1001 ± 47 MPa. From the microstructural analysis, the MTaC3 composition exhibited areas of uninfiltrated agglomeration that may decrease the TRS.

The fracture toughness of the baseline, MVC, MTaC3, and MTaC10 were measured and are listed in Table 4. Based on the previous mechanical results and microstructural analysis, the McBN composition was not tested for fracture toughness. The fracture toughness of the baseline composition was measured to be 20.7 ± 0.4 $MPa•m^{1/2}$. The fracture toughness of WC/Co composites with 54 vol % Co was reported to be in the range of 25.3 $MPa•m^{1/2}$ to 30.3 $MPa•m^{1/2}$.[17, 18] All measured compositions tested higher in fracture toughness than the baseline. The MTaC3 and MTaC10 compositions had fracture toughness values of 26.5 ± 0.3 $MPa•m^{1/2}$ and 23.1 ± 0.4 $MPa•m^{1/2}$, respectively. The MVC had a lower fracture toughness, 22.0 ± 0.5 $MPa•m^{1/2}$, than both TaC containing compositions; this trend has also been observed in the literature for WC-Co based MMCs.[2] More testing is recommended to determine the cause for the difference in fracture toughness between the two TaC containing compositions.

Based on the previous mechanical results and microstructural analysis, the cBN composition was not tested for wear resistance. The MTaC3 composition was also excluded due to the uninfiltrated agglomeration observed in the microstructure. The measured volume loss of the baseline composition was 20.8 ± 4.6 mm^3 after 4309 m of ASTM G65 Procedure A at 130 N applied load as shown in Table 5. Hong et al. measured a volume loss of of 7 mm^3 after 3000 m of a pin-on-disk test at 10 N applied load.[8] While the volume loss measured in this study was higher than that of Hong et al.

the difference in procedure makes a true comparison difficult. The volume loss of the MTaC10, and MVC are also listed in Table 5. Both the MTaC10 and MVC compositions had higher average volume loss than the baseline composition: 25.4 ± 3.5 mm^3 and 24.2 ± 1.2 mm^3, respectively. However, both the MTaC10 and MVC compositions tested within a standard deviation of the baseline composition. This was not unexpected for the MTaC10 composition as the measured hardness was also within a standard deviation of the baseline as previously discussed.

4. SUMMARY

Various WC/Cu-alloy based MMCs were manufactured using a pressureless infiltration technique in order to explore the effects of 10 vol% substitutions of VC, cBN, and TaC on the microstructure and mechanical properties. The MVC composite had areas of pullout caused in part by the VC embrittlement of the microstructure. The McBN composite was found to have pockets of agglomeration and porosity caused by the cBN particles not forming a strong bond with the metal matrix. The porosity area fraction in the McBN composite was measured to be 0.10, compared to the baseline of 0.01. The MTaC3 composition also showed areas of agglomeration, but had a considerably lower measured porosity area of fraction of 0.02. The cause for this difference in porosity was the partial infiltration of the TaC agglomerates. The MTaC10 composition also had a measured porosity area fraction of 0.02, while still containing some TaC agglomerates. However, the metal was able to infiltrate into the TaC agglomerates in the MTaC10 composites.

The baseline, MVC, and McBN compositions had a measured TRS of 838 ± 61 MPa, 743 ± 57 MPa, and 806 ± 23 MPa, respectively. As expected from microstructural

observations, the TRS and hardness of the MVC and McBN compositions tested below the baseline composition. However, both TaC containing compositions had a higher TRS than the baseline composition. The MTaC10 composition had a measured TRS of 1001 ± 47 MPa which was higher than the MTaC3 composition with a measured TRS of 847 ± 36. The difference in TRS between the two TaC containing compositions was likely due to the incomplete infiltration of the metal into the TaC agglomerates present in the MTaC3 composites. The baseline, MVC, MTaC3, and MTaC10 compositions had a measured fracture toughness of 20.7 ± 0.4 MPa•$m^{1/2}$, 22.0 ± 0.5 MPa•$m^{1/2}$, 26.5 ± 0.3 MPa•$m^{1/2}$, and 23.1 ± 0.4 MPa•$m^{1/2}$, respectively. The addition of VC and TaC both improved the fracture toughness in comparison to the baseline. The addition of VC and TaC increased the average volume loss in wear testing over the baseline. The average volume loss measurements for the baseline, MVC, and MTaC10 compositions were 20.8 ± 4.6 mm^3, 25.4 ± 3.5 mm^3 and 24.2 ± 1.2 mm^3, respectively. However, the difference between the average volume loss was not larger than the standard deviation for the measured compositions.

FIGURES AND TABLES

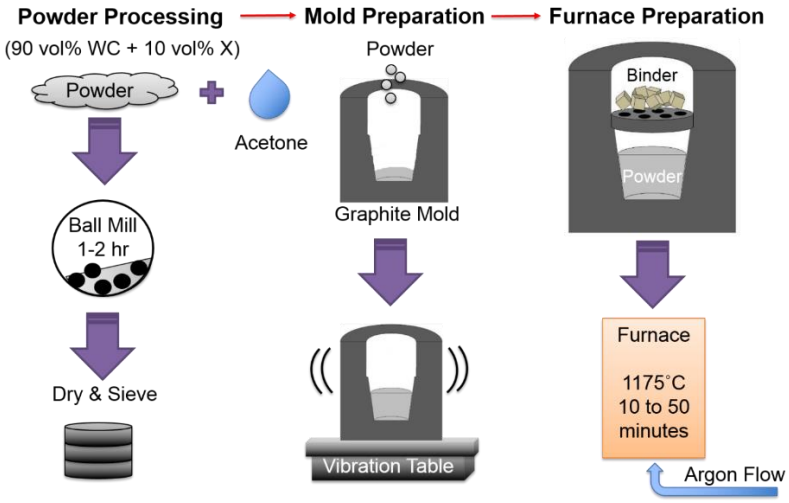

Figure 1. Processing process for various WC based MMC composites. Note that "X" denotes the secondary ceramic powder.

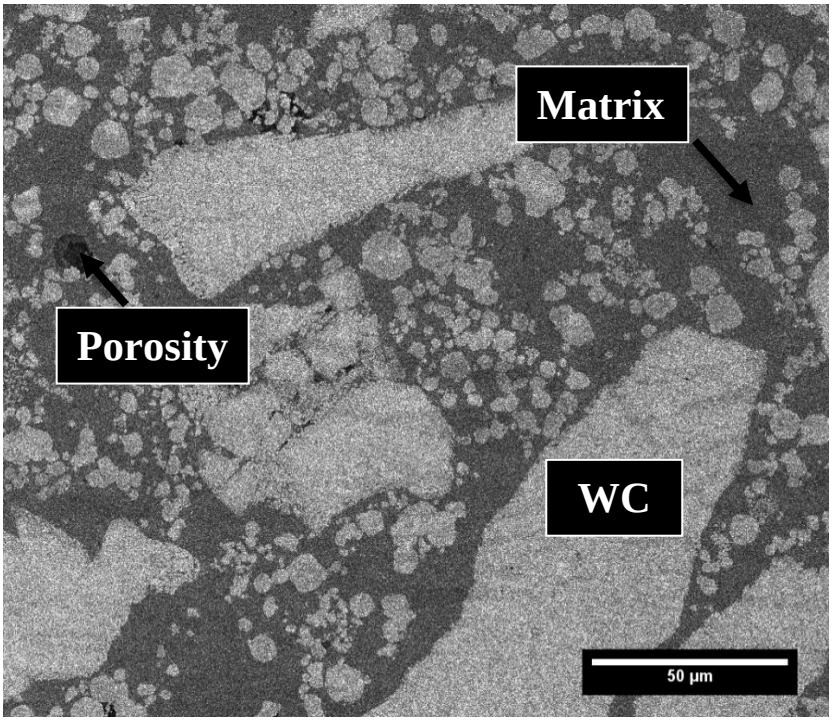

Figure 2. SEM micrograph showing the typical microstructure of the baseline composition.

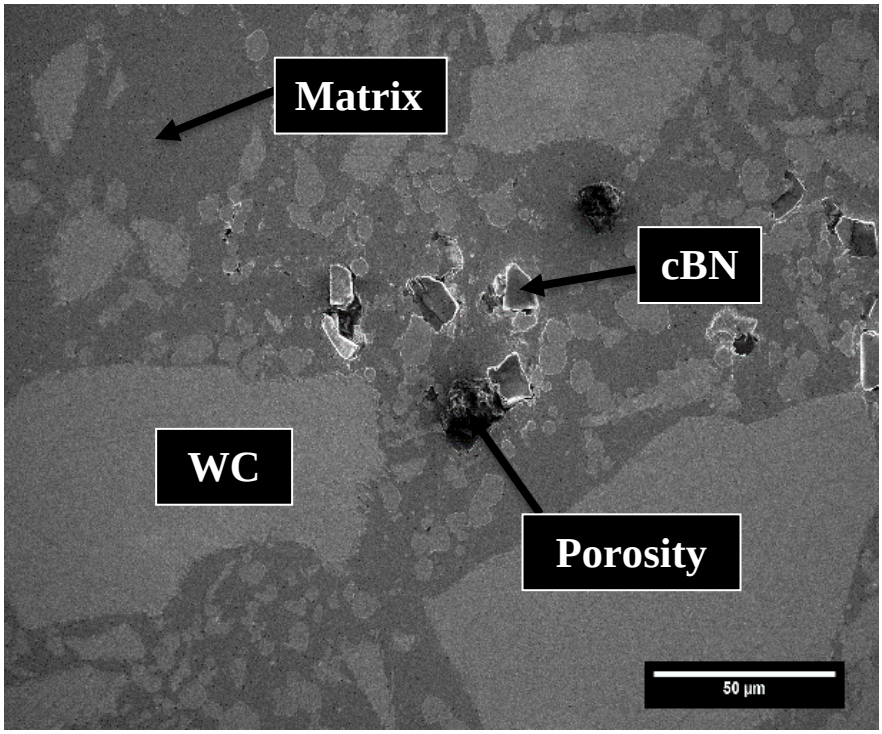

Figure 3. SEM micrograph of McBN, the cBN particles are agglomerated and are not chemically bonded to the matrix.

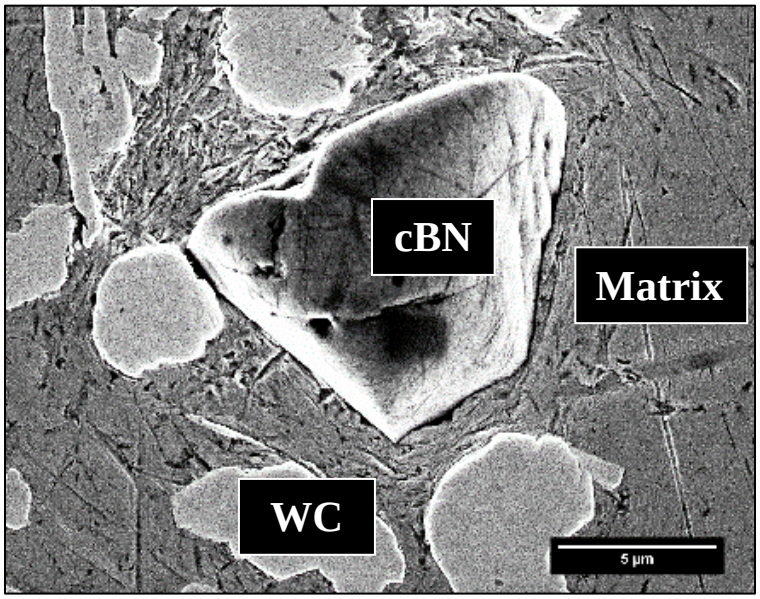

Figure 4. Close up of cBN particle in McBN composite. The particle appears to not be bonded to the metal.

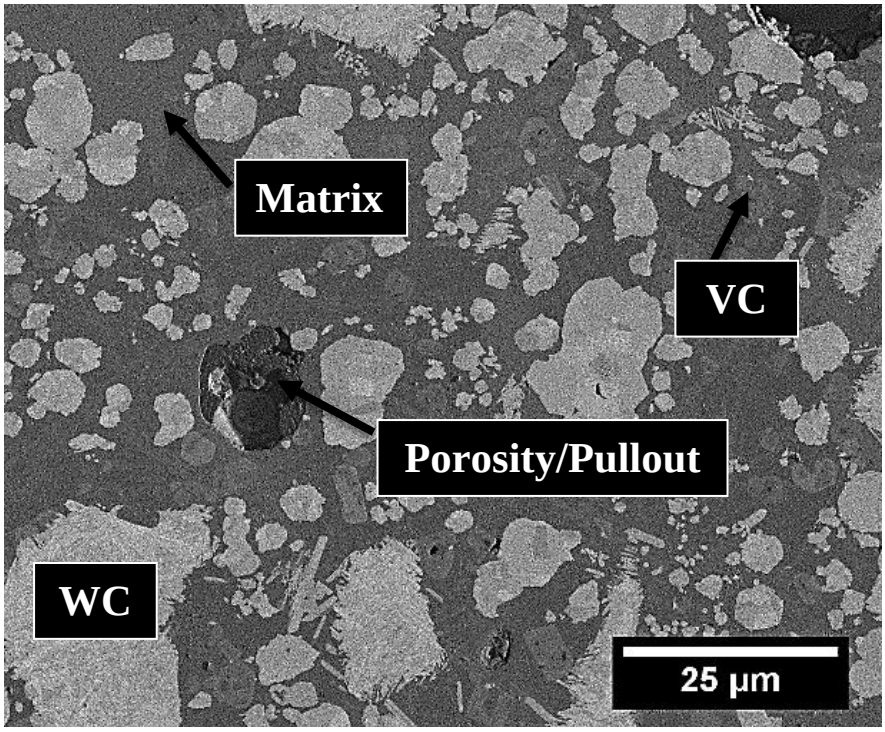

Figure 5. SEM micrograph of MVC, large areas of porosity may be caused by grain pullout.

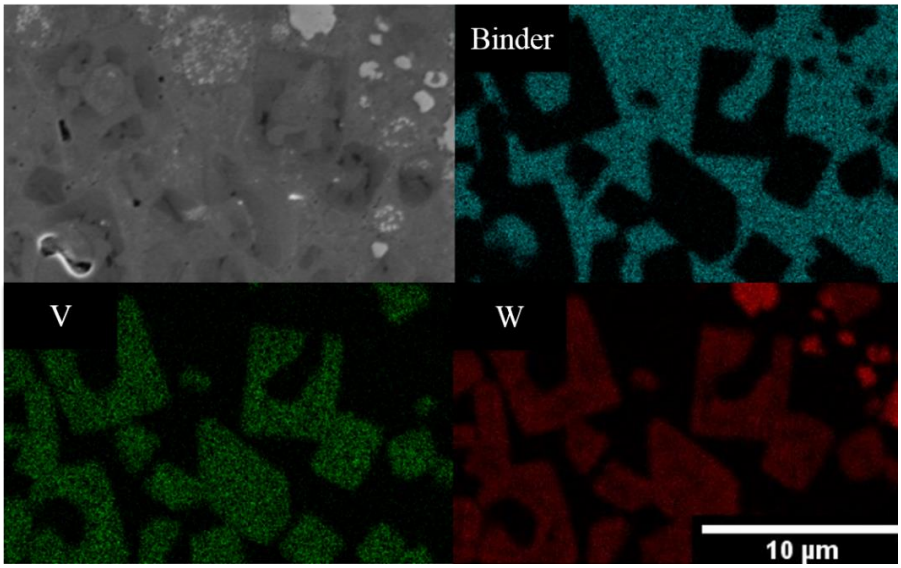

Figure 6. EDS micrograph of MVC microstructure (top left), binder (top right), vanadium (bottom left), and tungsten (bottom right). The areas of vanadium have tungsten in solid solution.

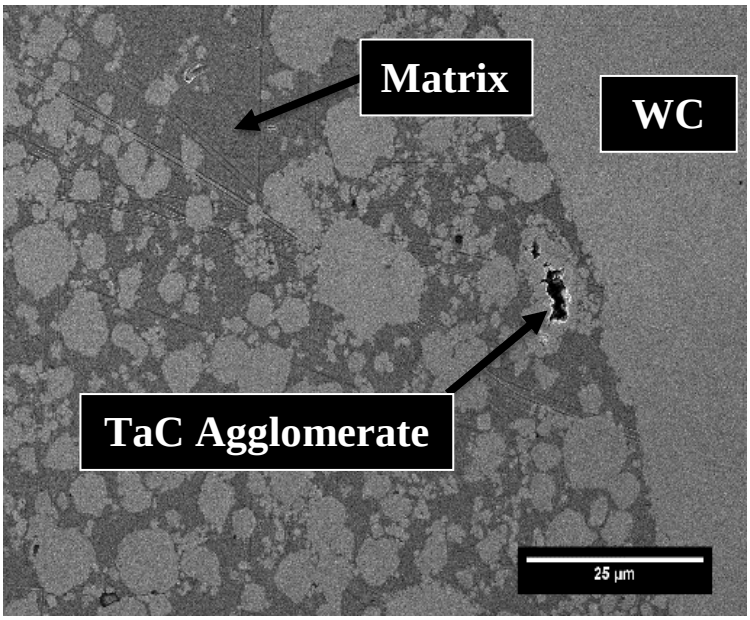

Figure 7. SEM micrograph of MTaC 3 µm. TaC agglomerates could not be fully infiltrated. The agglomerates were identified in light microscope where the contrast is different.

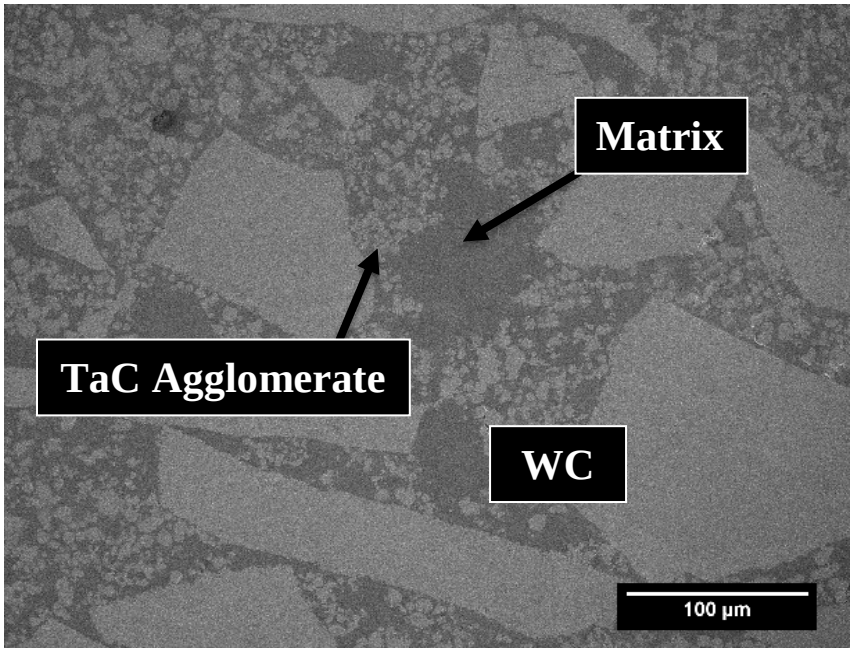

Figure 8. SEM micrograph of MTaC 10 µm. The TaC was shown not to agglomerate in a way that prevented full infiltration.

Table 1. Powder information and supplier for additives in various WC based MMCs.

Powder	Supplier	Particle Size (μm)
Vanadium Carbide	Atlantic Equipment Engineers (VA-301)	1-5
Cubic Boron Nitride	Engis Corporation	10-20
Tantalum Carbide	Inframat Advanced Materials (PN 73R-0601)	3
Tantalum Carbide	Atlantic Equipment Engineers (TA-301)	10

Table 2. Metal matrix composite designations, composition, and infiltration times at 1175°C.

MMC Designation	Powder Composition (vol%)					Infiltration Time (min)
	WC	VC	cBN	TaC (3 μm)	TaC (10 μm)	
Baseline	100	-	-	-	-	10
MVC	90	10	-	-	-	10
McBN	90	-	10	-	-	50
MTaC3	90	-	-	10	-	50
MTaC10	90	-	-	-	10	50

Table 3. Area fractions for ceramic particulate, metal binder, and porosity for various MMC compositions as determined by image analysis.

Composition	Area Fraction		
	Particulate	Porosity	Binder
Baseline	0.57	0.01	0.42
MVC	0.53	0.03*	0.44
McBN	0.38	0.10	0.52
MTaC3	0.54	0.02	0.44
MTaC10	0.58	0.02	0.40

*Includes Pullout

Table 4. Hardness, TRS, and fracture toughness were measured for the various MMCs.

Composition	Hardness (GPa)	Transverse Rupture Strength (MPa)	Fracture Toughness ($MPa•m^{1/2}$)
Baseline	3.3 ± 0.2	838 ± 61	20.7 ± 0.4
MVC	2.8 ± 0.2	743 ± 57	22.0 ± 0.5
McBN	2.8 ± 0.2	806 ± 23	-
MTaC3	3.3 ± 0.4	847 ± 36	26.5 ± 0.3
MTaC10	3.2 ± 0.2	1001 ± 47	23.1 ± 0.4

Table 5. ASTM G65 wear test measurements for selected composite compositions.

Tested Material	Volume Loss (mm^3)
Baseline	20.8 ± 4.6
MTaC10	25.4 ± 3.5
MVC	24.2 ± 1.2

REFERENCES

1. E. A. Almond, "Hardmetals," *Materials & Design*, 7[6] 324-29 (1986).

2. K. J. A. Brookes, "Hardmetals and Other Hard Materials." International Carbide Data: Hertfordshire UK, (1998).

3. G. S. Upadhyaya, "Materials science of cemented carbides — an overview," *Materials & Design,* 22[6] 483-89 (2001).

4. B. Wittmann, W.-D. Schubert, and B. Lux, "WC grain growth and grain growth inhibition in nickel and iron binder hardmetals," *Int. J. Refract. Met. Hard Mater.,* 20[1] 51-60 (2002).

5. A. R. Kennedy, J. D. Wood, and B. M. Weager, "The wetting and spontaneous infiltration of ceramics by molten copper," *Journal of Materials Science,* 35[12] 2909-12 (2000).

6. P. K. Deshpande and R. Y. Lin, "Wear resistance of WC particle reinforced copper matrix composites and the effect of porosity," *Materials Science and Engineering: A,* 418[1–2] 137-45 (2006).

7. P. K. Deshpande, J. H. Li, and R. Y. Lin, "Infrared processed Cu composites reinforced with WC particles," *Materials Science and Engineering: A,* 429[1–2] 58-65 (2006).

8. E. Hong, B. Kaplin, T. You, M.-s. Suh, Y.-S. Kim, and H. Choe, "Tribological properties of copper alloy-based composites reinforced with tungsten carbide particles," *Wear,* 270[9–10] 591-97 (2011).

9. ASTM B406-96, Standard Test Method for Transverse Rupture Strength of Cemented Carbides, ASTM International, West Conshohocken, PA, (2015).

10. ASTM C1327-15, Standard Test Method for Vickers Indentation Hardness of Advanced Ceramics, ASTM International, West Conshohocken, PA, (2015).

11. ASTM C1421-16, Standard Test Methods for Determination of Fracture Toughness of Advanced Ceramics at Ambient Temperature, ASTM International, West Conshohocken, PA, (2016).

12. S. Buckholz, "The influence of aluminum and carbon on the abrasion resistance of high manganese steels," *Masters Theses. 4471* (2013).

13. ASTM G65-16, Standard Test Method for Measuring Abrasion Using the Dry Sand/Rubber Wheel Apparatus, ASTM International, West Conshohocken, PA, (2016).
14. R. H. Wentorf Jr, "Cubic form of boron nitride," *The Journal of Chemical Physics,* 26[4] 956 (1957).

15. R. Shao, M. M. Krane, and K. Trumble, "Infiltration and directional solidification of CMSX-4 through a particulate ceramic preform," *MMTA,* 36[9] 2461-69 (2005).

16. K. Jia, T. E. Fischer, and B. Gallois, "Microstructure, hardness and toughness of nanostructured and conventional WC-Co composites," *Nanostruct. Mater.,* 10[5] 875-91 (1998).

17. A. Laptiev, Z. Pakiela, O. Tolochyn, and T. Brynk, "Microstructure and mechanical properties of WC-40Co composite obtained by impact sintering in solid state," *J. Alloys Compd.,* 687 135-42 (2016).

18. A. I. Tolochin, A. V. Laptev, M. E. Golovkova, and M. S. Koval'chenko, "Ultrafine high-cobalt VK40 hard alloy. I. Structure and properties," *Powder Metall. Met. Ceram.,* 47[3] 176-82 (2008).

SECTION

3. CONCLUSIONS

The research presented in this thesis focused on the wettability of Cu-Ni-Mn and Cu-Ni-Mn-Zn on various carbides, as well as the production of tungsten carbide based Cu-Ni-Mn-Zn metal matrix composites (MMCs). More specifically, this research focused on the baseline mechanical properties of tungsten carbide Cu-Ni-Mn-Zn and the changes in mechanical properties as 10 vol. % vanadium carbide (VC), cubic boron nitride (cBN), and tantalum carbide (TaC) was substituted for tungsten carbide (WC). This was done in an attempt to answer the questions that were presented in the Introduction section of this document. The procedures and results that were discussed in Paper I and Paper II were used to answer the questions accordingly:

1. *What other ceramic materials that have hardness ≥ 20 GPa are wet by Cu-Ni-Mn or Cu-Ni-Mn-Zn in a manner that would allow for spontaneous infiltration?*

The sessile drop method was used to determine the contact angles between two copper based alloys and substrates of TaC, WC, B_4C, and SiC. Both alloys wet the surfaces of the TaC, WC, and B_4C with contact angles lower than 70° which is a condition for spontaneous infiltration. The equilibrium contact angles at 1175°C for Cu-Ni-Mn-Zn on TaC, B_4C, and WC were measured to be 24°, 8°, and 0°, respectively. The equilibrium contact angles at 1175°C for Cu-Ni-Mn on TaC, B_4C, and WC were measured to be 47°, 13°, and 0°, respectively. The interfaces between both Cu-Ni-Mn-Zn and Cu-Ni-Mn and the TaC substrates showed no evidence of reaction products that would be expected to be harmful to continued wetting, thus making TaC a suitable

candidate for infiltration. The interfaces between both Cu-Ni-Mn-Zn and Cu-Ni-Mn and the WC substrates also showed no evidence of reaction products, thus making WC a suitable candidate for infiltration. Unfortunately, the interfaces between both Cu-Ni-Mn-Zn and Cu-Ni-Mn and the B_4C substrates showed evidence of the production of graphite which inhibited further wetting, which eliminated B_4C as a suitable candidate for infiltration.

Both alloys did not wet the surface of the SiC substrate. The contact angles of the Cu-Ni-Mn-Zn and Cu-Ni-Mn on the SiC substrate were measured to be 109° and 121°, respectively. Both of these contact angles were higher than 70° making SiC unsuitable for spontaneous infiltration. Furthermore, the reactions at the interface between SiC and both alloys produced graphite which inhibited further wetting.

2. *What are the baseline mechanical properties of tungsten carbide Cu-Ni-Mn-Zn MMCs produced by spontaneous infiltration?*

Several tungsten carbide Cu-Ni-Mn-Zn metal matrix composites were produced via spontaneous infiltration of a Cu-Ni-Mn-Zn alloy into a tungsten carbide powder bed at 1175°C. The microstructure was examined to ensure the successful infiltration of the composite. The resulting porosity of the microstructure was examined using area analysis and measured to be 1%. The baseline hardness was measured by Vickers indentation to be 3.3 ± 0.2 GPa. The baseline transverse rupture strength (TRS) was measured by three point bending to be 838 ± 61 MPa. The baseline fracture toughness was measured by chevron notch testing to be 20.7 ± 0.4 $MPa•m^{1/2}$. The wear resistance were measured using dry sliding on a silica abrasive wheel to be 20.8 ± 4.6 mm^3. A similar study

conducted by Hong et al. was used to compare the hardness and wear resistance. While the hardness values were shown to be in good agreement, the wear resistance values were difficult to compare because of the differences in methods of measurement.

3. *How does the substation of 10 vol. % tungsten carbide for vanadium carbide, cubic boron nitride, or tantalum carbide change the microstructure and mechanical properties of tungsten carbide Cu-Ni-Mn-Zn MMCs produced by spontaneous infiltration?*

Various WC-based Cu-Ni-Mn-Zn MMCs were produced by substituting 10 vol. % of the WC for VC, cBN, TaC 3μm (TaC3), and TaC 10μm (TaC10) for WC. The differences in microstructures were observed and compared to the baseline WC/Cu-Ni-Mn-Zn MMC. The VC substitution caused the embrittlement of the WC by creating a solid solution. This was shown by EDS and also by the presence of voids in the shape of WC particles in the microstructure that were likely caused by pullout. The cBN substitution increased the porosity area fraction measured in the microstructure to 0.10 in comparison to the baseline of 0.01. This increase was likely caused by the agglomeration in the cBN and the lack of a chemical bond between the metal and cBN resulting in poor infiltration into the agglomerates. The TaC3 substitution also caused poor infiltration into TaC agglomerates, but the difference in porosity area fraction in comparison to the baseline was only 0.01. The TaC was wet by the infiltrating alloy and thus did not have as much of an effect as cBN on the microstructure. The TaC10 substitution also resulted in agglomeration of the TaC, however the agglomerates that formed were able to be infiltrated by the Cu-Ni-Mn-Zn binder.

The VC containing MMCs tested lower than the baseline in hardness, TRS, with measured values of 2.8 ± 0.2 GPa and 743 ± 57 MPa, respectively. The cBN containing MMCs also tested lower than the baseline in hardness, TRS, with measured values of 2.8 ± 0.2 GPa and 806 ± 23 MPa, respectively. Both TaC containing MMCs had little effect on hardness and increased the TRS over the baseline with measured TRS of 847 ± 36 MPa for TaC3 and 1001 ± 47 for TaC10. The VC and TaC containing MMCs all tested higher than the baseline in fracture toughness with measured values of 22.0 ± 0.5 $MPa \bullet m^{1/2}$, 26.5 ± 0.3 $MPa \bullet m^{1/2}$, and 23.1 ± 0.4 $MPa \bullet m^{1/2}$ for VC, TaC3, and TaC10, respectively. However, both the VC and the TaC10 compositions had a higher volume loss than the baseline with measure values of 24.2 ± 1.2 mm^3 and 25.4 ± 3.5 mm^3, respectively.

4. FUTURE WORK

This research focuses on the processing and properties of tungsten carbide-based (WC-based) Cu-Ni-Mn-Zn metal matrix composites (MMCs) fabricated by pressureless infiltration. The first goal of this project was to test the wettability of Cu-Ni-Mn and Cu-Ni-Mn-Zn were tested using the sessile drop technique on several carbides to determine if they were suitable candidates for pressureless infiltration. The second goal of the project was to establish a baseline for the hardness, transverse rupture strength (TRS), fracture toughness, and wear resistance of WC/Cu-Ni-Mn-Zn MMCs and examine the effect of substituting 10 vol. % VC, cBN, TaC for WC on the microstructure and mechanical properties. During the course of this research, several areas that could be the subject of additional investigation arose. A few of which are:

1. The contact angles of Cu-Ni-Mn and Cu-Ni-Mn-Zn on B_4C were measured to be 13° and 8°, respectively. Though both angles were below 70° which is a requirement for pressureless infiltration[10], reactions at the interface produced graphite. Since graphite is not wet by either alloy this would likely prohibit infiltration. This provides the opportunity to coat B_4C powder in a material such as copper to influence the wetting characteristics of the system.[42] The chemistry of the metal could also be changed to influence the wetting characteristics of the system. A study by Froumin et al. showed that adding boron metal to copper can inhibit the dissociation of B_4C at the Cu/ B_4C interface.[73] These principals may also be applied to SiC by either adding a coating to SiC powder or adding Si to the alloy.

2. Many hard ceramic materials were used as additives to WC/Cu-Ni-Mn-Co with the most successful additive in terms of improvement of mechanical properties being TaC. A survey by Brookes has shown that Cr_3C_2 may also be of interest for the improvement of mechanical properties.[1] It was noted that Cr_3C_2 additions to WC/Co outperformed additions of TaC in terms of cost-effectiveness as well as overall performance.

3. What is the effect of Cu-Ni-Mn-Zn binder content on WC/Cu-Ni-Mn-Zn MMCs? It has been shown in the literature how varying the volume percent of Co changes the mechanical properties of WC/Co. [1, 4, 6] It would be valuable to learn if the effects of varying the Cu-Ni-Mn-Zn binder content yields a similar trend. Also there is room to study the particle size effect of the WC on the system. The literature also shows a substantial effect of particle size on the mechanical properties of WC/Co.[1, 6]

REFERENCES

1. K. J. A. Brookes, "Hardmetals and Other Hard Materials.″ International Carbide Data: Hertfordshire UK, (1998).

2. I. M. Hutchings, "Tribological properties of metal matrix composites," *Mater. Sci. Technol.,* 10[6] 513-17 (1994).

3. E. A. Almond, "Hardmetals," *Materials & Design,* 7[6] 324-29 (1986).

4. G. S. Upadhyaya, "Materials science of cemented carbides — an overview," *Materials & Design,* 22[6] 483-89 (2001).

5. W. C. Harrigan Jr, "1 - Metal Matrix Composites A2 - EVERETT, R.K," pp. 1-16. in Metal Matrix Composites: Processing and Interfaces**.** Edited by R. J. Arsenault. Academic Press, 1991.

6. A. Laptiev, Z. Pakiela, O. Tolochyn, and T. Brynk, "Microstructure and mechanical properties of WC-40Co composite obtained by impact sintering in solid state," *J. Alloys Compd.,* 687 135-42 (2016).

7. F. Delannay, L. Froyen, and A. Deruyttere, "The wetting of solids by molten metals and its relation to the preparation of metal-matrix composites composites," *Journal of Materials Science,* 22[1] 1-16 (1987).

8. G. V. Samsonov, A. D. Panasyuk, and G. K. Kozina, "Wetting of refractory carbides with liquid metals," *Soviet Powder Metallurgy and Metal Ceramics,* 7[11] 874-78 (1968).

9. N. Eustathopoulos, "Wetting by Liquid Metals—Application in Materials Processing: The Contribution of the Grenoble Group," *Metals,* 5[1] 350 (2015).

10. G. Kaptay and T. BÁrczy, "On the asymmetrical dependence of the threshold pressure of infiltration on the wettability of the porous solid by the infiltrating liquid," *Journal of Materials Science,* 40[9-10] 2531-35 (2005).

11. J. Bao, J. W. Newkirk, and S. Bao, "Wear-resistant WC composite hard coatings by brazing," *J. Mater. Eng. Perform.,* 13[4] 385-88 (2004).

12. E. Hong, B. Kaplin, T. You, M.-s. Suh, Y.-S. Kim, and H. Choe, "Tribological properties of copper alloy-based composites reinforced with tungsten carbide particles," *Wear,* 270[9–10] 591-97 (2011).

13. J. Liu, S. Yang, K. Liu, C. Gui, and W. Xia, "Effect of Age-Hardening Treatment on Microstructure and Sliding Wear-Resistance Performance of WC/Cu-Ni-Mn Composite Coatings," *MMTA,* 48[6] 3017-26 (2017).

14. P. Shaffer, "Materials Index.″ Plenum Press: New York, (1964).

15. V. N. Chuvil'deev, Y. V. Blagoveshchenskiy, A. V. Nokhrin, M. S. Boldin, N. V. Sakharov, N. V. Isaeva, S. V. Shotin, O. A. Belkin, A. A. Popov, E. S. Smirnova, and E. A. Lantsev, "Spark plasma sintering of tungsten carbide nanopowders obtained through DC arc plasma synthesis," *J. Alloys Compd.,* 708 547-61 (2017).

16. Y. Dong, L. Zhang, C. Wang, and Q. Shen, "In situ reactive synthesis and plasma-activated sintering of binderless WC ceramics," *Advances in Applied Ceramics,* 116[5] 267-71 (2017).

17. C. Liu, "The development and prospect of binderless carbide," *Materials China,* 35[8] 622-28 (2016).

18. A. R. Kennedy, J. D. Wood, and B. M. Weager, "The wetting and spontaneous infiltration of ceramics by molten copper," *Journal of Materials Science,* 35[12] 2909-12 (2000).

19. P. K. Deshpande, J. H. Li, and R. Y. Lin, "Infrared processed Cu composites reinforced with WC particles," *Materials Science and Engineering: A,* 429[1–2] 58-65 (2006).

20. B. Wittmann, W.-D. Schubert, and B. Lux, "WC grain growth and grain growth inhibition in nickel and iron binder hardmetals," *Int. J. Refract. Met. Hard Mater.,* 20[1] 51-60 (2002).

21. A. Kurlov and A. Gusev, "Tungsten Carbides Structure, Properties and Application in Hardmetals.″ Springer International Publishing: Switzerland, (2013).

22. X. Zhang, G. E. Hilmas, W. G. Fahrenholtz, and D. M. Deason, "Hot Pressing of Tantalum Carbide With and Without Sintering Additives," *J. Am. Ceram. Soc.,* 90[2] 393-401 (2007).

23. P. M. McKenna, "Tantalum Carbide its Relation to other Hard Refractory Compounds," *Industrial & Engineering Chemistry,* 28[7] 767-72 (1936).

24. S. A. Shvab and F. F. Egorov, "Structure and some properties of sintered tantalum carbide," *Soviet Powder Metallurgy and Metal Ceramics,* 21[11] 894-97 (1982).

25. F. Rezaei, M. G. Kakroudi, V. Shahedifar, N. P. Vafa, and M. Golrokhsari, "Densification, microstructure and mechanical properties of hot pressed tantalum carbide," *Ceram. Int.,* 43[4] 3489-94 (2017).

26. L. Lauter, R. Hochenauer, C. Buchegger, M. Bohn, and W. Lengauer, "Solid-state solubilities of grain-growth inhibitors in WC-Co and WC-MC-Co hardmetals," *J. Alloys Compd.,* 675 407-15 (2016).

27. W. S. Williams, "Transition-metal carbides," *Prog. Solid State Chem.,* 6 57-118 (1971).

28. M. Kaneko, T. Doshida, and K. Takai, "Changes in mechanical properties following cyclic prestressing of martensitic steel containing vanadium carbide in presence of nondiffusible hydrogen," *Materials Science and Engineering: A,* 674 375-83 (2016).

29. R. W. G. Wyckoff, "Crystal Structures Volume 2 Inorganic Compounds," Second ed. Vol. 2. John Wiley & Sons: New York, (1964).

30. G. E. Hollox, "Microstructure and mechanical behavior of carbides," *Materials Science and Engineering,* 3[3] 121-37 (1968).

31. H. R. Lee, D. J. Kim, N. M. Hwang, and D.-Y. Kim, "Role of Vanadium Carbide Additive during Sintering of WC–Co: Mechanism of Grain Growth Inhibition," *J. Am. Ceram. Soc.,* 86[1] 152-54 (2003).

32. R. G. Munro, "Material Properties of a Sintered α-SiC," *J. Phys. Chem. Ref. Data,* 26[5] 1195-203 (1997).

33. L. L. Snead, T. Nozawa, Y. Katoh, T.-S. Byun, S. Kondo, and D. A. Petti, "Handbook of SiC properties for fuel performance modeling," *J. Nucl. Mater.,* 371[1–3] 329-77 (2007).

34. Y.-M. Chiang, R. P. Messner, C. D. Terwilliger, and D. R. Behrendt, "Reaction-formed silicon carbide," *Materials Science and Engineering: A,* 144[1] 63-74 (1991).

35. X. Jing, X. Yang, D. Shi, and H. Niu, "Tensile creep behavior of three-dimensional four-step braided SiC/SiC composite at elevated temperature," *Ceram. Int.,* 43[9] 6721-29 (2017).

36. L. Teyssier, H. Maskrot, and L. Chaffron, "Simultaneous infiltration of submicron SiC powder and AHPCS during electrophoretic infiltration: A new straightforward process to synthetize SiCf/SiC composites," *J. Eur. Ceram. Soc.,* 36[6] 1359-64 (2016).

37. A. Onat, H. Akbulut, and F. Yilmaz, "Production and characterisation of silicon carbide particulate reinforced aluminium–copper alloy matrix composites by direct squeeze casting method," *J. Alloys Compd.,* 436[1–2] 375-82 (2007).
38. C. Rado, B. Drevet, and N. Eustathopoulos, "The role of compound formation in reactive wetting: the Cu/SiC system," *Acta Mater.,* 48[18–19] 4483-91 (2000).

39. C. Rado, S. Kalogeropoulou, and N. Eustathopoulos, "Wetting and bonding of Ni–Si alloys on silicon carbide," *Acta Mater.,* 47[2] 461-73 (1999).

40. G. W. Liu, M. L. Muolo, F. Valenza, and A. Passerone, "Survey on wetting of SiC by molten metals," *Ceram. Int.,* 36[4] 1177-88 (2010).

41. C. Ullner, A. Germak, H. Le Doussal, R. Morrell, T. Reich, and W. Vandermeulen, "Hardness testing on advanced technical ceramics," *J. Eur. Ceram. Soc.,* 21[4] 439-51 (2001).

42. T. Maruyama and S. Onose, "Fabrication and Thermal Conductivity of Boron Carbide/Copper Cermet," *J. Nucl. Sci. Technol.,* 36[4] 380-85 (1999).

43. F. Thévenot, "Boron carbide—A comprehensive review," *J. Eur. Ceram. Soc.,* 6[4] 205-25 (1990).

44. Q. Lin and R. Sui, "Wetting of B4C by molten Ni at 1753 K," *J. Alloys Compd.,* 556 274-79 (2013).

45. F. Thévenot, "Sintering of boron carbide and boron carbide-silicon carbide two-phase materials and their properties," *J. Nucl. Mater.,* 152[2] 154-62 (1988).

46. A. M. Turatti and A. S. Pereira, "Wear resistant boron carbide compacts produced by pressureless sintering," *Ceram. Int.,* 43[11] 7970-77 (2017).

47. X. Zhang, H. Gao, Z. Zhang, R. Wen, G. Wang, J. Mu, H. Che, and X. Zhang, "Effects of pressure on densification behaviour, microstructures and mechanical properties of boron carbide ceramics fabricated by hot pressing," *Ceram. Int.,* 43[8] 6345-52 (2017).

48. X. Du, Z. Zhang, Y. Wang, J. Wang, W. Wang, H. Wang, and Z. Fu, "Hot-Pressing Kinetics and Densification Mechanisms of Boron Carbide," *J. Am. Ceram. Soc.,* 98[5] 1400-06 (2015).

49. D. Patidar and R. S. Rana, "Effect of B4C particle reinforcement on the various properties of aluminium matrix composites: a survey paper," *Materials Today: Proceedings,* 4[2, Part A] 2981-88 (2017).

50. J. N. Panda, J. Bijwe, and R. K. Pandey, "Comparative potential assessment of solid lubricants on the performance of poly aryl ether ketone (PAEK) composites," *Wear,* 384–385 192-202 (2017).

51. R. H. Wentorf, "Synthesis of the Cubic Form of Boron Nitride," *The Journal of Chemical Physics,* 34[3] 809-12 (1961).

52. L. Vel, G. Demazeau, and J. Etourneau, "Cubic boron nitride: synthesis, physicochemical properties and applications," *Materials Science and Engineering: B,* 10[2] 149-64 (1991).

53. H. T. Hall, "Ultra-High-Pressure, High-Temperature Apparatus: the ``Belt"," *Rev. Sci. Instrum.,* 31[2] 125-31 (1960).

54. S.-T. Park, J.-G. Han, M. Keunecke, and K. Lee, "Mechanical and structural properties of multilayer c-BN coatings on cemented carbide cutting tools," *Int. J. Refract. Met. Hard Mater.,* 65 52-56 (2017).

55. K. E. Lindgren, A. Kauppi, and L. K. L. Falk, "Development of matrix microstructure in polycrystalline cubic boron nitride ceramics," *J. Eur. Ceram. Soc.,* 37[9] 3017-26 (2017).

56. R. Shao, M. M. Krane, and K. Trumble, "Infiltration and directional solidification of CMSX-4 through a particulate ceramic preform," *MMTA,* 36[9] 2461-69 (2005).

57. M. S. Greenfield, "Mine tools utilizing copper-manganese nickel brazing alloys." in. Google Patents, 1983.

58. R. M. Horton and R. A. Anthon, "Low melting point copper-manganese-zinc alloy for infiltration binder in matrix body rock drill bits." in. Google Patents, 1991.

59. E. G. Findeisen, Banerjee, Vivek Ranjan, Moll, Richard F., Kremmer, Siegmund, "Matrix powder for the production of bodies or components for wear-resistant applications and a component produced therefrom." in. WOKA Schweisstechnik GmbH, United States, 2004.

60. A. S. Mcdonald, C. W. Philp, and T. A. Sperakis, "Copper-zinc-manganese-nickel alloys." in. Google Patents, 1986.

61. T. Young, "An Essay on the Cohesion of Fluids," *Philos. Trans. R. Soc. London,* 95 65-87 (1805).

62. M. Humenik and W. D. Kingery, "Metal-Ceramic Interactions: III, Surface Tension and Wettability of Metal-Ceramic Systems," *J. Am. Ceram. Soc.,* 37[1] 18-23 (1954).

63. W. D. Kingery, "Metal-Ceramic Interactions:IV, Absolute Measurement of Metal-Ceramic Interfacial Energy and the Interfacial Adsorption of Silicon from Iron-Silicon Alloys," *J. Am. Ceram. Soc.,* 37[2] 42-45 (1954).

64. W. D. Kingery and M. Humenik, "Surface Tension at Elevated Temperatures. I. Furnace and Method for Use of the Sessile Drop Method; Surface Tension of Silicon, Iron and Nickel," *The Journal of Physical Chemistry,* 57[3] 359-63 (1953).

65. A. Sharma, "Relationship of thin film stability and morphology to macroscopic parameters of wetting in the apolar and polar systems," *Langmuir,* 9[3] 861-69 (1993).

66. B. Maruyama, E. V. Barrera, and L. Rabenberg, "8 - Characterization and Modification of Composite Interfaces A2 - EVERETT, R.K," pp. 181-216. in Metal Matrix Composites: Processing and Interfaces**.** Edited by R. J. Arsenault. Academic Press, 1991.

67. I. A. Aksay, C. E. Hoge, and J. A. Pask, "Wetting under chemical equilibrium and nonequilibrium conditions," *The Journal of Physical Chemistry*, 78[12] 1178-83 (1974).

68. A. B. D. Cassie and S. Baxter, "Wettability of porous surfaces," *Trans. Faraday Society,* 40[0] 546-51 (1944).

69. N. Eustathopoulos, R. Israel, B. Drevet, and D. Camel, "Reactive infiltration by Si: Infiltration versus wetting," *Scripta Mater.,* 62[12] 966-71 (2010).

70. L. Yin, B. T. Murray, and T. J. Singler, "Dissolutive wetting in the Bi–Sn system," *Acta Mater.,* 54[13] 3561-74 (2006).

71. F. Akhtar, S. J. Askari, K. A. Shah, X. Du, and S. Guo, "Microstructure, mechanical properties, electrical conductivity and wear behavior of high volume TiC reinforced Cu-matrix composites," *Mater. Charact.,* 60[4] 327-36 (2009).

72. P. Protsenko, O. Kozlova, R. Voytovych, and N. Eustathopoulos, "Dissolutive wetting of Si by molten Cu," *Journal of Materials Science,* 43[16] 5669-71 (2008).

73. N. Froumin, N. Frage, M. Aizenshtein, and M. P. Dariel, "Ceramic–metal interaction and wetting phenomena in the B4C/Cu system," *J. Eur. Ceram. Soc.,* 23[15] 2821-28 (2003).

74. E. O. Einset, "Capillary Infiltration Rates into Porous Media with Applications to Silcomp Processing," *J. Am. Ceram. Soc.,* 79[2] 333-38 (1996).
75. R. B. Bhagat, "3 - Casting Fiber-Reinforced Metal Matrix Composites A2 - EVERETT, R.K," pp. 43-82. in Metal Matrix Composites: Processing and Interfaces**.** Edited by R. J. Arsenault. Academic Press, 1991.

76. N. Frage, N. Froumin, M. Aizenshtein, L. Kutsenko, D. Fuks, and M. P. Dariel, "Reactive wetting in titanium carbide/non-reactive metal systems," *Curr. Opin. Solid State Mater. Sci.,* 9[4–5] 189-95 (2005).

77. N. Frage, N. Froumin, and M. P. Dariel, "Wetting of TiC by non-reactive liquid metals," *Acta Mater.,* 50[2] 237-45 (2002).

78. S. Tariolle, F. Thévenot, M. Aizenstein, M. P. Dariel, N. Frumin, and N. Frage, "Boron carbide–copper infiltrated cermets," *J. Solid State Chem.,* 177[2] 400-06 (2004).

79. A. Onat, "Mechanical and dry sliding wear properties of silicon carbide particulate reinforced aluminium–copper alloy matrix composites produced by direct squeeze casting method," *J. Alloys Compd.,* 489[1] 119-24 (2010).

80. S. C. Tjong and K. C. Lau, "Properties and abrasive wear of TiB2/Al-4%Cu composites produced by hot isostatic pressing," *Compos. Sci. Technol.,* 59[13] 2005-13 (1999).

81. C. R. Rambo, N. Travitzky, K. Zimmermann, and P. Greil, "Synthesis of TiC/Ti–Cu composites by pressureless reactive infiltration of TiCu alloy into carbon preforms fabricated by 3D-printing," *Mater. Lett.,* 59[8–9] 1028-31 (2005).

82. J. Bannan, R. I. Temple, and R. Jones, "In situ fabrication of titanium carbide reinforced copper MMC," *Mater. Sci. Technol.,* 19[8] 1148-50 (2003).

83. A. V. Smith and D. D. L. Chung, "Titanium diboride particle-reinforced aluminium with high wear resistance," *Journal of Materials Science,* 31[22] 5961-73 (1996).

84. K. P. Trumble, "Spontaneous infiltration of non-cylindrical porosity: Close-packed spheres," *Acta Mater.,* 46[7] 2363-67 (1998).

85. D. Lewis Iii, "6 - In Situ Reinforcement of Metal Matrix Composites A2 - EVERETT, R.K," pp. 121-50. in Metal Matrix Composites: Processing and Interfaces**.** Edited by R. J. Arsenault. Academic Press, 1991.

86. X. Luo, Y. Q. Yang, Y. C. Liu, Z. J. Ma, M. N. Yuan, and Y. Chen, "The fabrication and property of SiC fiber reinforced copper matrix composites," *Materials Science and Engineering: A,* 459[1–2] 244-50 (2007).

87. K. Jia, T. E. Fischer, and B. Gallois, "Microstructure, hardness and toughness of nanostructured and conventional WC-Co composites," *Nanostruct. Mater.,* 10[5] 875-91 (1998).

88. J. B. Quinn and G. D. Quinn, "Indentation brittleness of ceramics: a fresh approach," *Journal of Materials Science,* 32[16] 4331-46 (1997).

89. M. X. Gao, Y. Pan, F. J. Oliveira, J. L. Baptista, and J. M. Vieira, "Interpenetrating microstructure and fracture mechanism of NiAl/TiC composites by pressureless melt infiltration," *Mater. Lett.,* 58[11] 1761-65 (2004).

90. M. Koopman, K. K. Chawla, C. Coffin, B. R. Patterson, X. Deng, B. V. Patel, Z. Fang, and G. Lockwood, "Determination of elastic constants in WC/Co metal matrix composites by resonant ultrasound spectroscopy and impulse excitation," *Adv. Eng. Mater.,* 4[1-2] 37-42+5 (2002).

91. Z. Hashin and S. Shtrikman, "A variational approach to the theory of the elastic behaviour of multiphase materials," *J. Mech. Phys. Solids,* 11[2] 127-40 (1963).

92. A. J. Gant, M. G. Gee, and B. Roebuck, "Rotating wheel abrasion of WC/Co hardmetals," *Wear*, 258[1–4] 178-88 (2005).

93. ASTM G65-16, Standard Test Method for Measuring Abrasion Using the Dry Sand/Rubber Wheel Apparatus, ASTM International, West Conshohocken, PA, (2016).

94. W. Qiu, Y. Liu, J. Ye, H. Fan, and Y. Qiu, "Effects of (Ti,Ta,Nb,W)(C,N) on the microstructure, mechanical properties and corrosion behaviors of WC-Co cemented carbides," *Ceram. Int.*, 43[3] 2918-26 (2017).

VITA

Paul Brune was born on February 7th, 1992 in High Ridge, Missouri. He lived in High Ridge, Missouri before moving to Brinktown, Missouri in 2006 where he would attend high school at Maries County R1. Paul graduated high school in the spring of 2010 and moved to Rolla, Missouri to attend Missouri University of Science and Technology later that fall. By the fall semester of his sophomore year, he had declared his major to be Ceramic Engineering. During his four and a half years at Missouri S&T, Paul was a member of the Missouri Gamma Chapter of the Sigma Phi Epsilon Fraternity. In the spring of his sophomore year he joined the KERAMOS chapter of Missouri S&T. Through KERAMOS, Paul was able to travel to Washington D.C. twice, first to talk to congressmen and congresswomen about the importance of STEM funding and again to represent Missouri S&T at the National Science Fair alongside good friends and mentors. During his undergraduate career, Paul worked for KOHLER as a co-op and GE Aviation as a summer intern. Paul received his B.S. degree in Ceramic Engineering from Missouri University of Science and Technology in December of 2014.

Paul began his graduate work as a masters student for Dr. Gregory E. Hilmas at the Missouri University of Science and Technology in January of 2015. During his graduate career, Paul focused his research on the processing and properties of tungsten carbide copper-based metal matrix composites. He also assisted with the mechanical properties lab, gave presentations at PowderMet 2016, published two papers, and taught lessons in mechanical properties of ceramics and thermal properties of ceramics. Paul received his M.S. degree in Ceramic Engineering from Missouri University of Science and Technology in July of 2017.